THE FLORIDA STATE UNIVERSITY

COLLEGE OF ARTS AND SCIENCES

ENSO FIDELITY IN TWO COUPLED MODELS

By

J-P MICHAEL

A Thesis submitted to the
Department of Earth, Ocean and Atmospheric Science
in partial fulfillment of the
requirements for the degree of
Master of Science

Degree Awarded:
Fall Semester, 2010

The members of the committee approve the thesis of J-P Michael defended on August 31, 2010.

Eric Chassignet

Professor Co-Directing Thesis

Vasu Misra

Professor Co-Directing Thesis

Zhaohua Wu

Committee Member

Approved:

Lynn Dudley, Chair, Department of Earth, Ocean and Atmospheric Science

---

Joseph Travis, Dean, College of Arts and Sciences

The Graduate School has verified and approved the above-named committee members.

TABLE OF CONTENTS

LIST OF FIGURES

ABSTRACT

This study examines the fidelity of the ENSO simulation in two coupled model integrations and compares this with available global ocean data assimilation. The two models are CAM-HYCOM coupled model developed by the HYCOM Consortium and CCSM3.0. The difference between the two climate models is in the use of different ocean general circulation model (OGCM). The hybrid isopycnal-sigma-pressure coordinate ocean model Hybrid Coordinate Ocean Model (HYCOM) replaces the ocean model Parallel Ocean Program (POP) of the CCSM3.0. In both, the atmospheric general circulation model (AGCM) Community Atmosphere Model (CAM) is used. In this way the coupled systems are compared in a controlled setting so that the effects of the OGCM may be obtained. Henceforth the two models will be referred to as CAM-HYCOM and CAM-POP respectively.

Comparison of 200 years of model output is used discarding the first 100 years to account for spin-up issues. Both models (CAM-HYCOM and CAM-POP) are compared to observational data for duration, intensity, and global impacts of ENSO. Based on the analysis of equatorial SST, thermocline depth, wind stress and precipitation, ENSO in the CAM-HYCOM model is weaker and farther east than observations while CAM-POP is zonal and extends west of the international dateline. CAM-POP also has an erroneous biennial cycle of the equatorial pacific SSTs. The analysis of the subsurface ocean advective terms highlights the problems of the model simulations.

CHAPTER 1

INTRODUCTION

1.1 Defining ENSO

The trade winds are one of the most persistent climatological features of the earth. These easterly winds, which exist over much of the global tropics, are also the driving force for equatorial ocean currents. Although the phenomenon of the trade winds has been known for hundreds of years, the relationship between them and ocean has become known only during the past century and may still not be completely understood. The trades converge near the equator at the Intertropical Convergence Zone (ITCZ) where warm moist air rises (Philander 1990). In the Pacific, convection occurs primarily in the west over the warm pool as shown in Fig. 1.1.

The term "trade" originally meant "track" or "path," referring to the constant path of the trade winds. The intensity, however, of the wind along this track is not constant. When the trade winds over the Pacific are strong enough, the Western Pacific stays warmer than the Eastern Pacific. In the absence of strong winds the current weakens. The existence of a temperature gradient in the Equatorial Pacific in a weaker-than-normal trade-wind regime allows the equatorial counter current to dominate, deepening the thermocline in the east, and submerging cold waters below the level of upwelling. In turn, surface temperature the Eastern Pacific rise—the

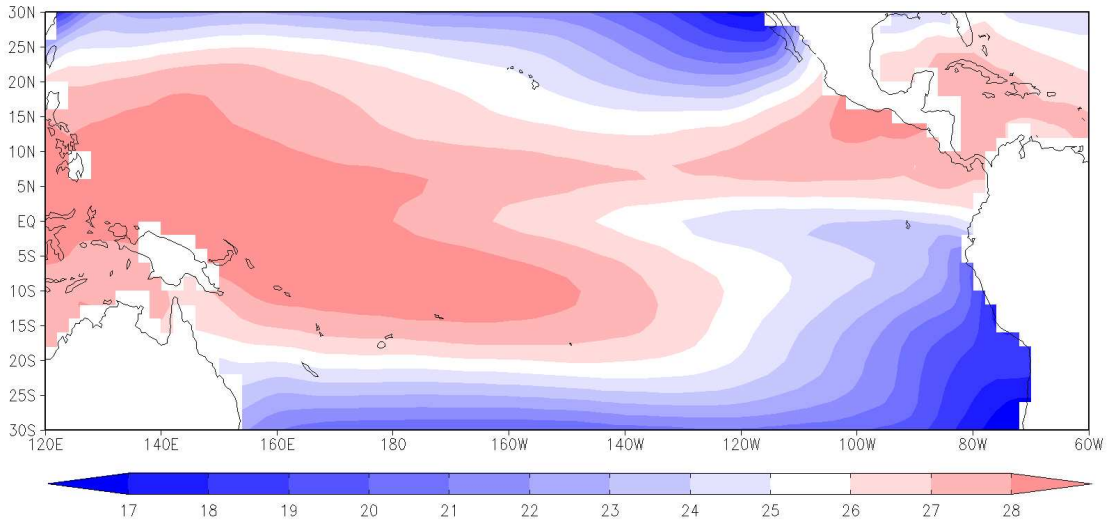

Figure 1.1: Average sea surface temperatures in the Equatorial Pacific.

phenomenon known as El Niño. The reverse, cooling in the Eastern Pacific, is known as La Niña. Coincident with this pattern of warming and cooling (El Niño and La Niña) is the pressure variation between Darwin, Australia, and Tahiti in the South Pacific Ocean that is known as the Southern Oscillation. Together the two phenomena are called El Niño–Southern Oscillation (ENSO).

Methods of quantifying ENSO phase and strength have expanded as our understanding and the observational network have grown. Two of the earliest metrics used to quantify ENSO are the sea surface temperature (SST) anomalies off the coast of Peru (Niño Index) and the difference in sea level pressure between Darwin, Australia, and Tahiti (Southern Oscillation Index, or SOI). Initially, it was not known that warming off the coast of Peru extended thousands of kilometers west. Until the 1960s El Niño events were recorded only in the waters near Peru (Philander 1990). As late as the 1980s many ENSO definitions still focused primarily on the SSTs along the coast of South America (Trenberth 1997). This area is now known as the Niño 1+2

region (see Fig. 1.2). Several problems exist with the Niño 1+2 time series. First, this region has a weak response to cold events. Additionally, warm phases occasionally arise without significant change of SST in the coastal region—a phenomenon that seems to be occurring more often in recent years (Yu and Kao 2007).

As understanding of ENSO increased, so did the methods of quantifying it. Today, the larger Niño regions 3, 4, and 3.4, which tend to have less noise than Niño 1+2, are more commonly used in defining ENSO events. The Niño 4 has a weak response to warm events and the Niño 3 has the strongest correlation with SOI. Additionally, the Japan Meteorological Agency (JMA) uses a region similar to Niño 3, but confined to 4 degrees from the equator to define the JMA index. Newer methods include combining ENSO metrics [e.g. the Multivariate ENSO Index (MEI) and the Trans–Niño Index (TNI)] or using statistical methods. Weare (1986) defines an index using the first Principal Component (PC) of the Equatorial Pacific SST Empirical Orthogonal Function (EOF). The Niño 3, 3.4, and the SOI are the most widely used indices in operational meteorology in the United States. The National Weather Service (NWS) retrospectively defines ENSO events by the three-month running average SST in Niño 3.4 region. The NWS determines warm (cold) events as any period with of at least five consecutive months with temperatures 0.5^0C above (below) normal. For the SOI, negative (positive) values indicate warm (cold) phase. Each measurement of ENSO has limitations, but each demarcates warm and cold events of ENSO nearly unanimously; only the weakest events are sometimes contested. Furthermore, most indices are well correlated with each other (above .9 in some instances), so the choice of index usually depends on the preference of the author. The reader is referred to Hanley et al. (2003) for a more detailed discussion on ENSO indices.

These methods of quantifying ENSO do not sufficiently describe how meridional or zonal the area of anomalous SSTs is and whether the event is located in the Central

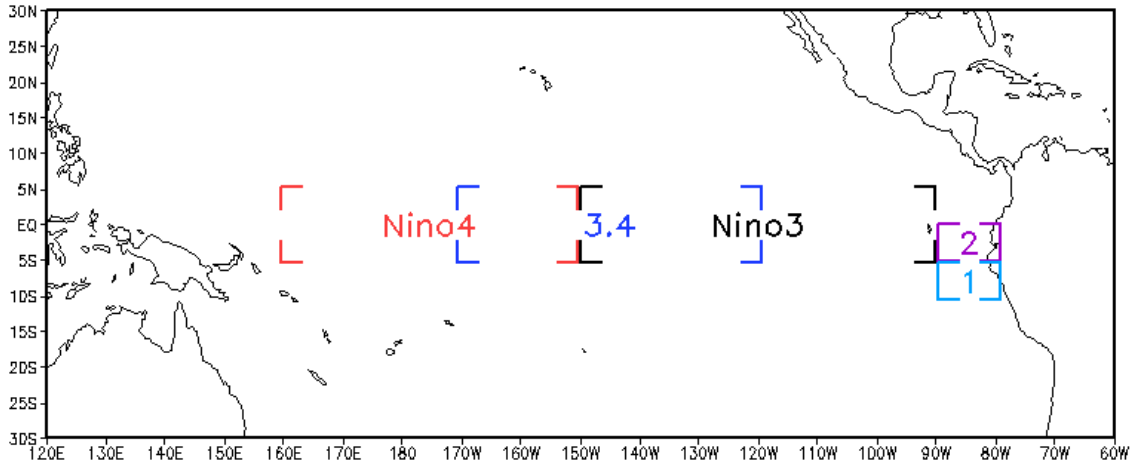

Figure 1.2: Regions used to determine Niño Indices.

or Eastern Pacific. Since 2007, research into variations involving eastern Pacific warm (EPW) events and central Pacific warm (CPW) events has become an active research topic. Variance of the EPW, the more familiar type of warm event, peeks in the Niño 3 region and will be explained in the following sections. The CPW, often dubbed "Modoki" ENSO [Modoki is a Japanese word meaning "a similar but different thing" (Ashok et al. 2007)] peeks in the Niño 3.4 and Niño 4 regions (Kao and Yu 2009). Generally, an event with a larger maximum anomaly will also have a larger spatial structure; however, the area of warming is not stationary. Some indices may be better suited for phase onsets but miss the maximum anomaly. For this reason, this paper will examine the typical structure associated with the ENSO event to best analyze the performance of the models.

1.2 ENSO Teleconnections

ENSO teleconnections have been the primary basis for seasonal to interannual climate prediction. Droughts in Brazil and Indonesia and cooler and wetter conditions

in the Southeast United States are likely when El Niño is present; the reverse pattern is expected in these areas during a La Niña episode (Diaz et al. 2001, Glantz 2000). It should be noted that the strength of the ENSO event can impact these global teleconnections nonlinearly. In addition, the location of the event (EPW versus CPW) can drastically change the climatological teleconnections. For example, Kim et al. (2009) found that the tracks of tropical storms in the North Atlantic Basin make landfall more often during CPW than during EPW. The number of named storms in the Atlantic hurricane season also rises during cold events and declines during EPW events.

The most prominent feature associated with the warm phase of ENSO is a dry anomaly wrapping around the area of warming in the eastern Pacific extending to the north- and southeast from the Western Equatorial Pacific. This anomalous "horseshoe" pattern is produced by the convective branch of the Walker cell being displaced eastward from Indonesia to the open ocean. There is anomalous precipitation over the unusually warm equatorial waters. This pattern can be seen in Fig. 1.3. Another striking feature is the rain in coastal Peru where, normally, there is little rain. During the cold phase, the convective branch of the Walker circulation strengthens and the "horseshoe" pattern is anomalously wet. Fig. 1.4 shows robust temperature ENSO teleconnections for both warm and cold events.

North American winters are heavily influenced by the warm and cold phases of ENSO. The Southeast United States experiences a cooler and wetter winter during the warm phase and a warmer and drier winter during the cold phase. Likewise, the northwestern portion of the continent has a milder winter during the warm phase and a colder winter during the cold phase. The ENSO-related shift of the Polar Jet over the Pacific and the North American continent is responsible for these changes (Glantz 2000).

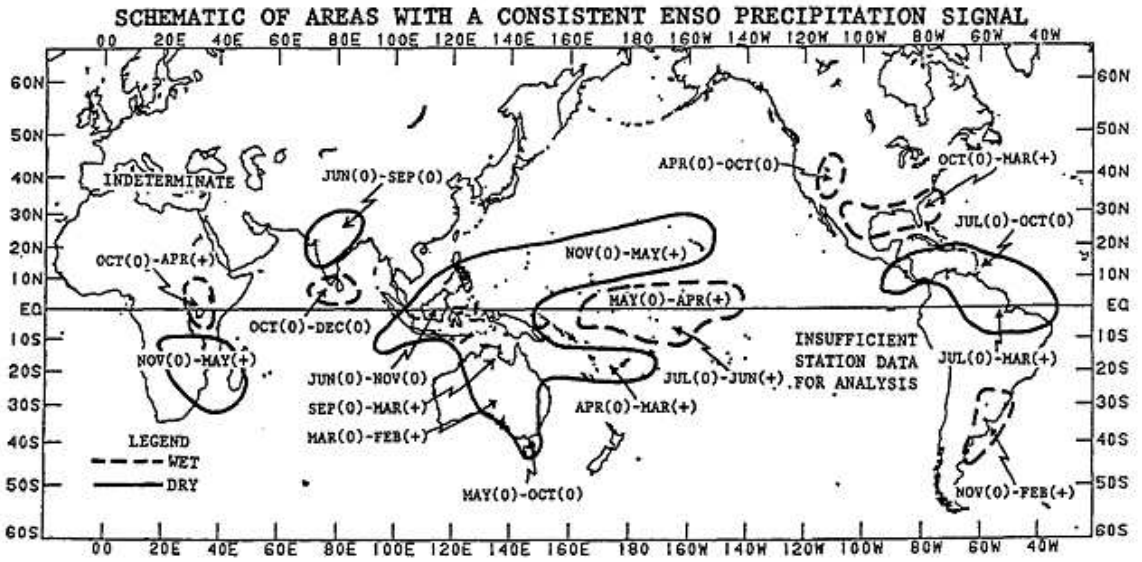

Figure 1.3: Schematic representation of the principal ENSO precipitation teleconnections. From Ropelewki and Halpert (1987).

The situation in North America during the summer is much different. During boreal summer, the North American continental climate has a much lower correlation to the ENSO index. Yet, a significant effect is felt from the changes in the seasonal tropical cyclone (TC) activity in the Atlantic basin (Gray 1984). During a warm phase there is less TC activity due to increased vertical shear in the TC development region that inhibits the strengthening of storms. A cold ENSO phase acts to reduce the amount of shear and more TC's are observed in cold years. Tang and Neelin (2004) have shown that the onset period of a warm phase can also alter TC activity. If the nonneutral phase begins at the start of a hurricane season, then the adjustment from neutral to warm (cold) causes the troposphere over the TC development region to be more (less) stable than it is during a neutral year, thus acting to diminish (promote) TC activity for several months. In a more recent paper, Kim et al. (2009) show that anomalous climatological global circulation associated with EPW and CPW causes a

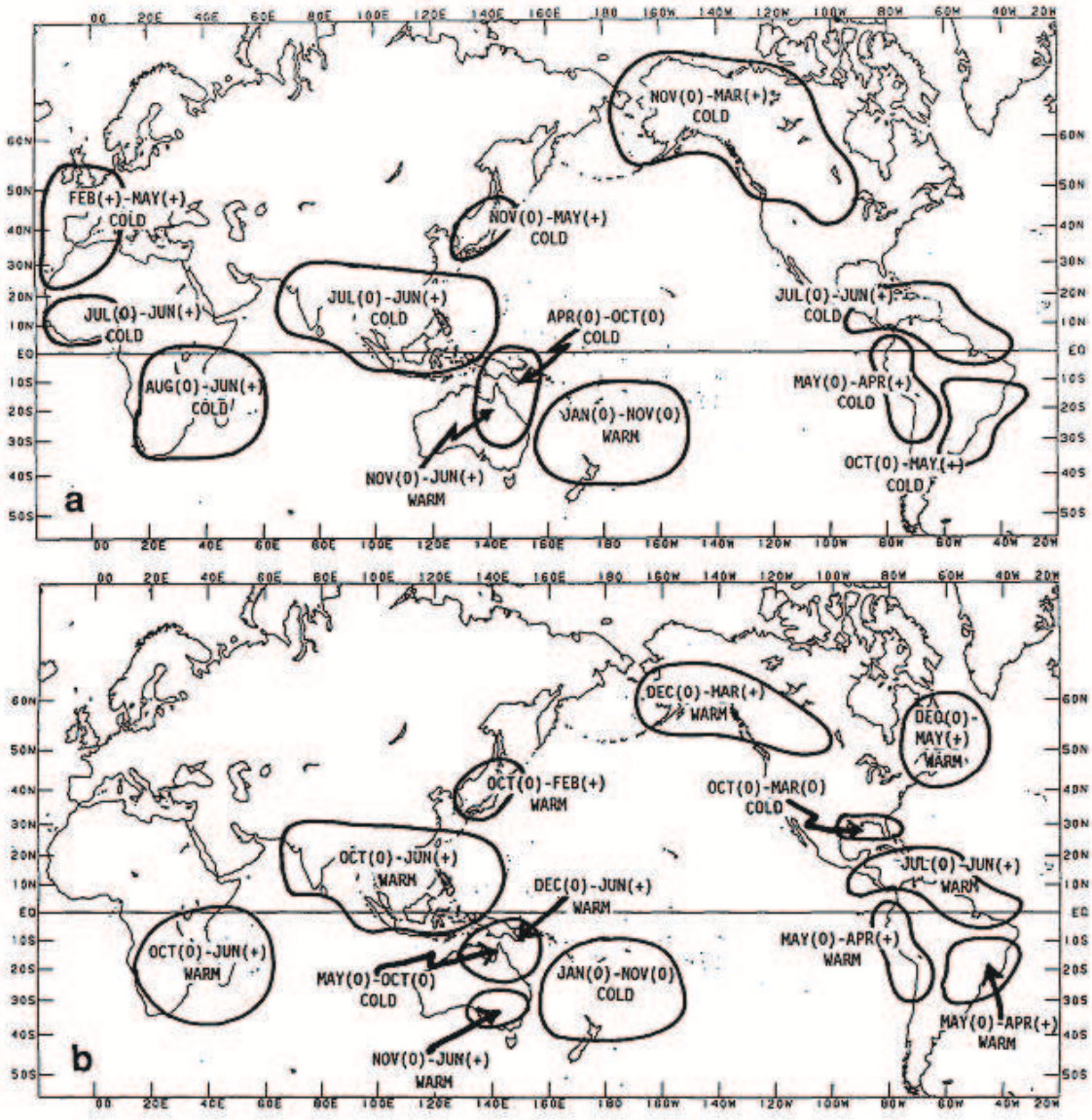

Figure 1.4: Schematic representation of the principal ENSO temperature teleconnections for (a) cold (b) warm. From Halpert and Ropelewki (1992).

large difference in the number of landfalling TCs. In the case where warming occurs in the Eastern Pacific, the effect is a reduction in storms. If the warming is located in the Central Pacific, then the TC tracks in that hurricane season will more likely make landfall over the continental United States.

Whereas the conclusions about teleconnections discussed thus far have been based on observations, Hoerling and Kumar (2002) used model output to construct a more thorough outline of the teleconnections. The results were categorized as (a) weak, moderate, and strong events and (b) West, Central, and East Pacific events to illustrate the nonlinear relationships between ENSO forcing and regional climates.

In accordance with the North American teleconnections described above, modeled conditions in the northwest are drier during a weaker warm ENSO phase (Hoerling and Kumar 2002). It might be assumed that the stronger the warm anomaly, the drier conditions in this region would be. However, it was found that for moderate and strong warm phases, the Pacific storm track takes a different route and causes more precipitation in California rather than less. In the model, the cool–wet relationship in the Southeast United States does prove to have a more linear relationship with increasingly stronger warm events. The location of the warm event (either West, Central, and East Pacific) does not have a linear relationship with the climate of the South East United States. Contrary to the precipitation relationship implied by the TC tracks discussed in Kim et al. (2009), the Southern United States is drier during Central Pacific warm events in the model. This shows that improvements to the models are still needed to make seasonal predictions confidently. The role of one key model element, the ocean simulation, is investigated in Chapter 3.

1.3 Biological and Economic Effects of ENSO

Understanding and simulating ENSO is of primary importance in climate modeling because of the far-reaching biological and economic implications. One of the most important effects ENSO has on the planet is the noticeable ecological shifts that occur in response to either a warm or a cold phase. These changes in local ecosystems when coupled with human interaction can affect species survival in a particular region. For example, overfishing in a region alone can lead to species reduction and when combined with a change in fish population related to ENSO phase near extinction has been observed for several species(Barber and Chavez 1983). Near or total extinction of a species is a tragedy, and the economic impact can be the permanent dismantling of a regional industry. Agriculture is also often a victim when an extreme unanticipated ENSO event occurs. When crops fail, great social and economic strife can follow.

To understand how ENSO can affect the biological realm so profoundly requires looking at the basic physical process that leads to the change in ecosystem. For the coast of Peru, the resulting change in ecosystem alters the phytoplankton population which then causes proportional changes in fish, bird, and marine mammal populations (Barber and Chavez 1983).

The phytoplankton in the Eastern Equatorial Pacific live within the mixed layer of the ocean on a combination of sunlight (which decreases exponentially from the surface downward) and nutrient rich water (which reaches surface from below the thermocline via upwelling). During a warm event, sunlight and nutrients are less available to the phytoplankton. Near the coast of Peru, winds favorable for coastal upwelling are still present during the warm phase (and may actually be stronger). Nutrients are absent during this phase because the depth of the thermocline has increased to a level below the depth of entrainment. As a result the upwelling is not transporting as much nutrient-rich water to the surface. Second, less sunlight will

reach the bottom of the mixed layer because the thickness of the mixed layer has also increased during the warm phase (Cane 1983) and sunlight decreases rapidly through seawater. Since the phytoplankton are roughly uniformly distributed in the mixed layer the amount of sunlight reaching any given phytoplankton is reduced and so the population is smaller. Less phytoplankton in this region leads to less biomass for higher organisms.

The reduction of phytoplankton is felt profoundly in higher tropic organisms as well. In the El Niño of 1982, arguably the strongest warm phase ever, the absence of fish, birds, and seals was extensively documented. In the anomalous currents some species of sea life, such as shrimp, simply drift from their normal habitat with no apparent change in population. For others, such as anchovy, the 20-fold reduction of their primary food source decreased their growth, survival rate, and reproductive fitness. The severity of the 1982 El Niño had such profound effects on anchovy that concentrated schools near the coast were found with numerous dead anchovies—an occurrence not observed in any of the recent past warm events. The jack mackerel were equally affected by the 1982 event. Due to the changing environment and diminished food source, the mackerel, usually seen offshore, moved into a tight 30-km band along shore. The increased density allowed predatory fish and fisherman to nearly eradicate the mackerel (Barber and Chavez 1983). The Galapagos fur seal was also gravely impacted. Due to the reduction of fish, adult seals were less successful at finding food. Observations show that adult females stayed at sea for about 5 days (3.5 days longer than normal) and returned with too little milk to feed their pups. The effects of the 1982 event were strong enough to kill not only the majority of pups, but also many adults (Pauly et al. 1989).

The reduction of multiple fish species during a warm phase is not isolated to the equatorial region. Near Christmas Island the disappearance of small fish and squid

caused the blue-faced booby and great frigate bird to abandon nests on the island. In June 1982 the number of great frigate birds was 20,000; by November, the number was fewer than 100. Because of the relatively long lifespan of the birds, the parent s can abandon the baby birds and attempt to survive on the reduced food supply. Keeping the babies would jeopardize the survival of the flock by forcing competition for too little food. However, the magnitude of the 1982 event caused many of the adults to perish (Schreiber and Schreiber 1984).

The marked biological effects of ENSO also have important economic implications that compel us to continue ENSO prediction studies. The impact on the South American fishing industry is apparent from the discussion above; however, there are far-reaching global effects on agriculture and other sectors as well. From the 1940s to the 1980s guano from Peruvian seabirds was in great demand for use as fertilizer in Europe and the United States, creating a large industry in Peru (Glantz 2000). In this case, the reduction in seabird populations near Peru, due to El Niño, reduces the production of guano.

Today, agriculture is much less dependent on guano, but the effects of ENSO on the industry are still present. Changes in seasonal rainfall in the Southeastern United States related to ENSO are a key influence on agriculture in that region. For instance, in the Southeastern states, crops such as corn and tobacco, which are sensitive to precipitation, are significantly affected by ENSO (Hansen et al. 1998). Interestingly, the failure of the fishing season due to warm ENSO events may also impact crops planted in the Southeast United States. In years when demand for fish is high, the price of livestock feed, which contains fish protein, increases. In response to this increase in price and demand of livestock feed, soybean farmers tend to plant more soybeans, which can substitute for fish protein, 2 years after warm events (Hansen et al. 1998).

Accurate seasonal climate predictions can inform decision makers on when and where to plant crops. Being forewarned about the nature of upcoming ENSO events can not only protect farmers from crop failures but can also help farmers choose crops that may be in higher demand. During warm event winters, the prices of bell peppers and snap beans increase. The increase in hard-freezes for the South East United States reduces crop yields of winter-harvest vegetables. In Florida, diminished efficacy of fertilizers and damaged plant roots results from the excess rainfall during El Niño years. Because Florida is the primary producer of winter-harvest bell peppers and snap beans, farmers in regions outside Florida with mild winters can capitalize on this shortage (Hansen et al. 1999).

1.4 ENSO Theory

The first three sections of this chapter cover the definition of ENSO and the ramifications it has on the planet. A simple introductory explanation of the cause of ENSO was also given. The basis for setting off ENSO events is related to changes in the trade winds leading to a positive feedback. This section will explain the physical mechanism which causes the observed cycle which repeats irregularly every 2-7 years.

Currently, there are two primary ENSO theories acknowledged by the scientific community. The first, Delayed Oscillator Theory (DOT) (Suarez and Schopf 1988), explains ENSO in terms of equatorial Kelvin and Rossby waves in the Pacific Ocean. The second, Recharge-Discharge Theory (Jin 1997), explains ENSO in terms of Sverdrup transport of warm water volume in the ocean. Other than these two paradigms of ENSO there are several other theories used to describe the air-sea interactions responsible for ENSO. For example, Wang (2001) put forth a unified theory which combined all the leading contemporary theories of ENSO into one unified theory.

The discussion provided here will focus on DOT and recharge-discharge oscillator in coupled models.

The underling principal of DOT (Suarez and Schopf 1988) is that perturbations in zonal wind stress in the Central Equatorial Pacific will generate Equatorial Kelvin and Rossby waves. These waves propagate zonally and displace the thermocline vertically as they travel across the Pacific Basin. To the east of the wind stress anomaly, Kelvin waves move toward the eastern boundary, the western coast of South America, and then partially reflect back to the west as Rossby waves. Likewise, to the west of the wind stress anomaly, equatorial Rossby waves travel west to the eventually reflect back as Kelvin waves.

Action of these waves to displace the thermocline vertically (either upwelling or downwelling) depends on the sign of the wind stress anomaly. If the anomaly is positive (an eastward anomaly), the Kelvin wave will downwell the thermocline creating a positive SST anomaly in the Eastern Pacific and the initial Rossby wave will up upwell in the West Pacific. If the anomaly is westward, the initial waves will lead to a cold ENSO phase. Upon reflection, the upwelling/downwelling waves reach opposite edge the Pacific Ocean and reverse the SST anomaly that was originally created.

The time scale for the Kelvin waves and Rossby wave to cause a change in SST in the Pacific Ocean is much less than the observed return period of ENSO. For the speed of Kelvin waves and the length of the Pacific Ocean it takes about one month for a Kelvin wave generated in the Central Pacific to reach the eastern boundary. Rossby waves, moving a one third the speed of Kelvin waves, require three months to reach the western boundary. Thus, it takes approximately four months delay time for the reflected waves to reach the Central Pacific - much shorter than the observed ENSO period.

Since Suarez and Schopf (1988), there have been many modifications and suggested

improvements to the DOT which help explain the return period of ENSO better. Neelin (1991) proposed that instead of one wave propagating away from the Central Pacific, multiple waves propagated as a train and the cumulative effect altered the SSTs in the Eastern Pacific. This was later replaced by the Schneider et al. (1995) which proposed that off-equatorial Rossby waves interacted with the equatorial Kelvin waves to slow the process.

As shown in Jin (1997), the ENSO oscillations can be explained by the time evolution of the equatorial sea-surface temperatures (SST) and the thermocline depth. To begin, the basic state of the thermocline can be expressed in terms of the depth in the East and depth in the West Pacific and the zonal wind stress along the equator. At the equator, wind stress anomalies to the west will drive the thermocline to be deeper in the west and shallower in the east. Conversely, a westerly anomaly will shoal the thermocline in the west and deepen it in the east. From this we get the following relationship (note that a westerly anomaly of zonal wind stress is negative):

$$h_E = h_W + \hat{\tau}$$

where h_E is the anomalous depth of the eastern Pacific thermocline, h_W is the anomalous depth of the Western Pacific thermocline, and $\hat{\tau}$ is proportional to the zonal averaged wind stress.

Next, we examine the slow adjustment process to the average thermocline depth anomalies in the Western Pacific related to ENSO. For this we generalize the forcing into two groups: damping (due to energy loss, mixing, currents, etc.) and wind forcing (largely proportional to the anomalous zonal wind stress $\hat{\tau}$). As stated previously, a westerly wind stress anomaly will case the thermocline in the west to shoal. Letting r represent the slow damping rate in the system we get:

$$\frac{dh_W}{dt} = -rh_W - \alpha\hat{\tau}$$

Likewise, we can describe the time evolution of the Equatorial Pacific SSTs by three forcings: a damping rate, anomalous wind forcing, and the anomalous vertical thermal gradient of the upper ocean. We will form the tendency equation for the Eastern Equatorial Pacific. We know that as the thermocline deepens in the east, upwelling will bring less cold water to the surface, so the tendency is forced proportionally to h_E. As the trade winds slack in the east, SST tendency is also positively forced because there will be less Ekman pumping bringing cooler water to the surface and also less evaporative cooling. We choose c, γ, and δ_S as the coefficients of the system:

$$\frac{dT_E}{dt} = -cT_E + \gamma h_E + \delta_S \tau_E$$

where τ_E is the average wind stress over the Eastern Pacific.

The equations derived so far are a fine approximation for the slow changing system of ENSO but are still not simple enough to form a paradigm for the oscillation. For this, we must consider the atmospheric response to SST anomalies. Jin (1997) makes the following assumption to close the system:

$$\hat{\tau} = bT_E,\ \tau_E = b'T_e$$

where b and b' are coupling coefficients.

This relationship is based on the observed atmospheric response to changes in SSTs in which warmer Eastern Equatorial Pacific SSTs cause anomalous westerlies over most of the Equatorial Pacific (with a westerly anomaly to the west and easterly

anomaly to the east of the SST anomaly). Thus b is somewhat larger than b'.

We get two equations in terms of western thermocline depth anomaly and eastern SST anomaly:

$$\frac{dT_E}{dt} = -cT_E + \gamma(h_W + (bT_E)) + \delta_S(b'T_e)$$

$$\text{let} \quad R = \gamma b + \delta_S b' - c$$

$$\frac{dh_W}{dt} = -rh_W - \alpha b T_E \tag{1.1}$$

$$\frac{dT_E}{dt} = RT_E + \gamma h_W \tag{1.2}$$

Equations 1.1 and 1.2 describe the time evolution of ENSO; the earlier derived equations can be used to get values for wind stress and thermocline in the east. Fig. 1.5 shows the four phases derived from this system. Starting from an initial neutral state, we can see that a small SST anomaly will lead to growth of the anomaly based on the equations above. This will result in basin-averaged positive wind stress anomalies, which, from the very first relationship made, will result in a deeper thermocline in the east and a shallow thermocline in the west. This is the height of the discharge phase as the Sverdrup transport out of the equator is at a maximum. This result is shown in Fig. 1.5 (a). From here, the negative h_W will act to reduce the SST anomaly in the east. At present, h_W and T_E in equation 1.1 will counteract, fixing the depth of the thermocline in the west. Simultaneously, the wind stress is returning to normal strength. The sum of these interactions leads to a normal SST and wind stress but an anomalous shallow thermocline across the Equatorial Pacific as shown in of Fig. 1.5 (b). The anomalous shallow thermocline is also the phase with the lowest warm water volume in the Equatorial Pacific—the "discharge" of warm water has taken place.

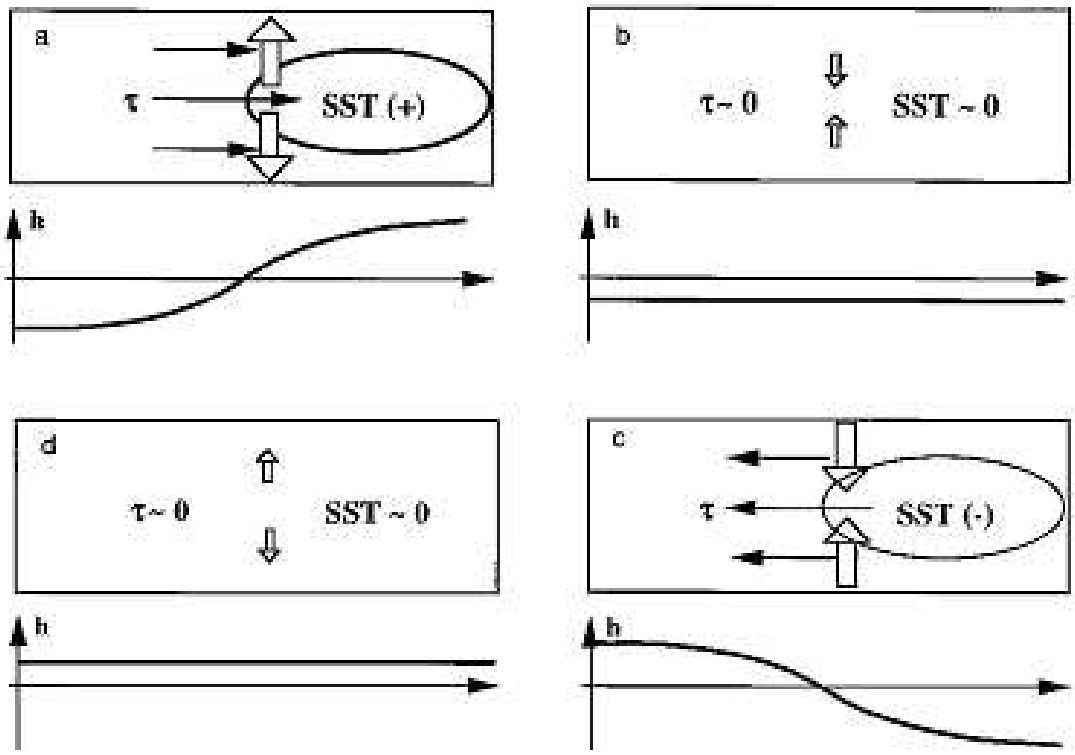

Figure 1.5: Schematic of the fours phases of the recharge-discharge oscillation a) warm phase b) warm to cold transition phase c) cold phase and d) cold to warm transition phase. The rectangular box represents the Equatorial Pacific basin; the elliptical circle represents the SST anomaly; the thin filled arrows represent wind stress anomaly; the thick unfilled arrows represent the recharge/discharge of equatorial heat content; the graph below each box shows the distrobution of the thermocline depth anomaly. Copied from Jin (1997).

The warm water will tend to recharge in the equatorial region. This is accomplished by a slow return to quasi-equilibrium. The neutral wind stress causes the tilt of the thermocline to tend toward normal conditions. SSTs in the Equatorial Pacific continue to cool due to the upwelling of anomalous cold water in the subsurface ocean. As the SSTs cool below normal levels, anomalous easterlies develop that further force the SSTs down because of enhanced upwelling and evaporative cooling. The strengthened trades cause an influx of warm water near the surface and tilt the thermocline beyond normal conditions. The result is the mature cold phase of ENSO as shown in Fig. 1.5 (c). Finally, the increased depth of the thermocline in the west causes a return to normal SSTs as shown in equation 1.1. Physically, this is due to the recharge of warm water volume in the Equatorial Pacific. As the warm water volume returns, the anomalous upwelling gradually advects less cold water to the surface and the SSTs return to normal. This response also weakens the trades back to normal levels. However, the thermocline is deeper over the whole Equatorial Pacific; the "recharge" of warm water has concluded. The ocean conditions are ready for the onset of another warm phase to begin. It has been shown that warm phases do not follow the recharge phase as this model might suggest. The reasons for this are beyond the scope of this paper.

A fundamental property of ENSO is the apparent phase-locking of ENSO to the seasonal cycle (Rasmusson and Carpenter 1982). This phenomenon is often referred to as to the spring persistence barrier or the spring predictability barrier because in April and May a large drop in the persistence causes poor model prediction of ENSO. The phase-locking of ENSO can be observed most readily as the peak of ENSO events tends to occur at the end of a calendar year.

To understand the mechanism for this phase-locking, the seasonal propagation of the anomalous trade winds needs to be identified. During an ENSO event, the

changes in the Walker circulation lead to anomalous convection in the Western Pacific and anomalous winds over the Central Equatorial Pacific. Because of the change in the solar angle throughout the year, the latitude of these anomalies shifts south in January-March as the peak solar radiation moves south of the equator (Clarke 2008). Gadgil et al. (1984) showed that when SSTs reach 28°, convection can occur. So as the water south of the equator warms, the convection shifts southward causing wind anomalies to do the same.

The propagation of the anomalous winds southward at the beginning of the calendar year removes the positive feedback of ENSO. For instance, during a warm event the anomalous westerlies allow the SSTs in the Eastern Pacific to warm. As this anomaly moves south, the thermocline depth begins to shoal and SSTs cool in the East Equatorial Pacific thus ending the warm phase. Therefore, the demise of ENSO events is significantly phase locked to the seasonal cycle even though these events do not always occur at regular intervals.

1.5 Modeling ENSO

Prior to coupled climate modeling, work with ENSO was limited. As demonstrated in section 4, the interannual warming and cooling in the Equatorial Pacific is due to interactions between the atmosphere and ocean and so a free-running uncoupled atmospheric or ocean model will not produce ENSO variability. Early work in modeling ENSO was based on forcing the atmosphere with some prescribed SSTs resembling a warm or cold event. This produced an atmospheric response that allowed scientists to study the effects of ENSO (Hoerling et al. 1997) but did not allow for atmospheric feedback to the ocean and the natural evolution of SSTs.

Coupling the ocean and atmosphere allows for the feedbacks necessary to produce

ENSO but does not ensure that ENSO variability will occur. Since even the most state-of-the-art models contain biases, coupling the atmospheric general circulation model (AGCM) and the ocean general circulation model (OGCM) forces each component with values containing the model bias of the other. This is less than ideal when trying to reproduce a feature of the real climate, which depends heavily on these interactions. The result of coupling becomes dependent on the "tuning" of the model to some degree. Today, there are climate models capable of producing features resembling ENSO, however, even some of the world's flagship climate models, those used by the Intergovernmental Panel on Climate Change (IPCC) for the fourth assessment report (AR4), lack ENSO variability.

Because ENSO is a coupled atmosphere-ocean phenomenon, ENSO simulation requires a fully coupled general circulation model (GCM). In a fully coupled system, small biases in the ocean model will produce bias in the atmospheric model. The inherent bias on the atmospheric model plus the ocean forcing bias feeds back to the ocean model and so on. The result is that coupled models with some similarity to observed ENSO are still deficient in a number of ways.

The relative strength of ENSO variance for coupled GCMs (CGCMs) that have ENSO is sometimes as little as half or as much as twice the strength observed. One of the models used in this study, CCSM3.0 (also referred to as CAM-POP for this study) is considered to have acceptable strength of ENSO. Depending on the measurement of ENSO, some studies measure CAM-POP's ENSO amplitude to be either a too weak (Guilyardi et al. 2009) or too strong (Neale et al. 2008). This study will show that the variability of CAM-POP is mostly biennial in nature; the variance explained by the mechanism for ENSO is too weak.

Another common bias of modeled ENSO is for the return period to be too fast (higher frequency) or too regular. As stated earlier the observed return period is 2-7

years. In CAM-POP the return period is both too quick (2 years) and too regular; the tendency of contemporary models to have ENSO events occurring at regular intervals is common (Guilyiardi 2006). Neale et al. (2008) studied the biases of CAM-POP ENSO simulation in detail; improvements to the convection scheme used resulted in a better ENSO simulation for CAM-POP.

Relevant to the physical process is the seasonal cycle of wind forcing. In some models, the seasonal cycle behaves in a completely different manner than observed. Often these models have little or no ENSO variability. Some models, however, do not have a seasonal cycle, which, by theory, would produce ENSO events yet still have ENSO variability. CAM-POP is an example of such a model; this deviation from theory would lead the investigators to ask whether the model has a true ENSO component.

Other pertinent features of ENSO include the spatial structure of ENSO events measured by SSTs, the tilt of the thermocline, and the precipitation anomalies over the tropical Pacific. Most CGCMs tend to extend the variance of SSTs west beyond the date line where variance is observed to end. CAM-POP extends ENSO events beyond the date line but does so to a lesser extent than some of the other AR4 models. The tilt of the thermocline is measured by the anomalous depth across the Equatorial Pacific basin, which can be described as a see-saw pivoting at 160^{o} W. Generally, models capture the pivoting with biases in the location of the pivot point or the meridional extent of variance (Capotondi et al. 2006). The AR4 models' precipitation anomalies are often zonally distributed compared to the observed anomalous Walker circulation. Likewise, CAM-POP exhibits positive precipitation anomalies over the entire Equatorial Pacific in response to ENSO events (Joseph and Nigam 2006); this is a error not likely to be corrected by improvements to the OCGM.

The problem with using fully coupled GCMs is that they are so complex the

physics is not easily understood (Clarke 2008). Making even small changes to a model can dramatically change the ENSO properties; as will be shown in this study, changing the OGCM does just that. Additionally, "tuning" of model parameters can sometimes yield better looking results without any improvement of model physics. This makes it even more difficult to determine what is physically responsible for the ENSO variability and how to address the model biases.

1.6 Outline

The research preformed in this study includes analysis of ENSO characteristics observed in the atmosphere and Pacific upper ocean. Analysis will follow mostly from Misra et al. (2007) and Misra et al. (2008). Several analysis techniques (regression analysis, spectral analysis, and others) are employed to describe the performance of CAM-HYCOM and CAM-POP in terms of statistically significant observed ENSO features. A new data analysis method, ensemble empirical mode decomposition (EEMD), is used to examine the ENSO oscillation beyond traditional methods.

Chapter 2 of this paper will provide information on the analysis datasets used, variables derived, and the methodology followed for analyzing CAM-HYCOM and CAM-POP. Chapter 3 will discuss how well CAM-HYCOM and CAM-POP simulate ENSO and how consistent they are with ENSO theory. ENSO features examined are return period, seasonal phase-locking, spatial structure, the oceanic teleconnections, the atmospheric teleconnections, and dynamics. Chapter 4 will summarize the results and provide conclusions.

CHAPTER 2

DATA AND METHODOLOGY

2.1 Data Sets

This study aims to deduce the effects of two different ocean models [Hybrid Coordinate Model (HYCOM) and Parallel Ocean Model (POP)] on simulation of ENSO in a coupled climate model system. Both ocean models, HYCOM and POP, are coupled to the same atmospheric, land, and sea ice models. Both models have the same resolution and are run from the same initial conditions using similar model setting. By holding all other experimental variables fixed, the effects of the ocean model can be extracted from the results. Data for the CAM AGCM coupled to POP OGCM (CAM-POP) model is available from the NCAR Climate System Modeling group NCAR Community Climate System Model 3.0 (CCSM3.0) downloaded from Earth System Grid (URL: http://www.earthsystemgrid.org/home.htm model) run b30.004. In this study, the medium resolution configuration with spectral resolution T42 (approximately 2.8 degree resolution) is used for both models. For both ocean models, the North Pole is displaced over Greenland and the latitudinal resolution is curvilinear with finer at the equator. POP has a vertical resolution of 40 levels with finer resolution near the surface. The hybrid coordinates in HYCOM are configured with 36 levels. The CAM-HYCOM coupled model was developed by the HYCOM

Consortium by Alan Wallcraft and Ge Peng; it was run by Dr. Jianjun Yin at the Center for Oceanic and Atmospheric Prediction Studies (COAPS). Because it takes centuries to develop ocean currents from a motionless state in OGCMs, before coupling the OGCM to the ACGM, the OGCM was coupled with climatological forcing until an equilibrium state was reached. This process is known as "spin-up." After the OGCM reaches equilibrium, the OGCM is coupled to the full GCM. The sudden change from a climatologically forced system to a fully coupled system produces a shock to the ocean known as initialization shock. Recovery after initialization shock is much quicker than the initial spin up; within a few decades the coupled system reaches an equilibrium state whereas initial ocean spin-up takes centuries. In order to circumvent variability associated with initialization shock, 200 years of model integration were used starting with year 101. At the time of this study, 300 years of the CAM-HYCOM model integration were complete.

As a baseline for comparison, Extended Reconstruction Sea Surface Temperature version 3b (ERSST) (Smith et al. 2008), NCEP-NCAR Reanalysis (NCEP-NCAR) (Kalnay et al. 1996), Global Data Assimilation System (GODAS) (Behringer and Xue 2004), and Climate Forecast System twentieth century control run (CFS) (Saha et al. 2006) are used. Horizontal resolution is 2^{o} for ERSST and 2.5^{o} for NCEP-NCAR. GODAS has 1^{o} longitudinal resolution, 0.5^{o} latitudinal resolution, and 10 meter vertical resolution in the upper ocean.

Pacific SSTs are represented by 100 years of the ERSST from January 1909 to December 2008. There are two convincing arguments against using 100 years of SSTs. The first argument is that ENSO has changes in mode and nature since the mid-1970's Allan et al. (1996) and that these changes may be the result of increased greenhouse gases (GHG) Trenberth and Hoar (1996). This implies that the later years should not be used to compare with pre-industrial model runs. The second argument favors

using the more recent years. Prior to the satellite era, the climate records of the equatorial Pacific are sparse. Both arguments challenge the usefulness of all available data. Fortunately, this study does not attempt to differentiate between the nuances of ENSO variability before and after the industrial era or to match model output exactly to observations but rather measures the general performance of the two models. For this reason, the inclusion of 100 years is more desirable because it increases confidence in the results while providing a paradigm of how models should operate.

As a baseline for comparison, Extended Reconstruction Sea Surface Temperature version 3b (ERSST) (Smith et al. 2008), NCEP-NCAR Reanalysis (NCEP-NCAR) (Kalnay et al. 1996), Global Data Assimilation System (GODAS) (Behringer and Xue 2004), and Climate Forecast System twentieth century control run (CFS) (Saha et al. 2006) are used. Horizontal resolution is 2° for ERSST and 2.5° for NCEP-NCAR. GODAS has 1° longitudinal resolution, 0.5° latitudinal resolution, and 10 meter vertical resolution in the upper ocean. The reason these datasets were chosen will be explained briefly.

Pacific SSTs are represented by 100 years of the ERSST from January 1909 to December 2008. There are two convincing arguments against using 100 years of SSTs. The first argument is that ENSO has changes in mode and nature since the mid-1970's Allan et al. (1996) and that these changes may be the result of increased greenhouse gases (GHG) Trenberth and Hoar (1996). This implies that the later years should not be used to compare with pre-industrial model runs. The second argument favors using the more recent years. Prior to the satellite era, the climate records of the equatorial Pacific are sparse. Both arguments challenge the usefulness of all available data. This study does not attempt to differentiate between the nuances of ENSO variability before and after the industrial era or to match model output exactly to observations but rather measures the general performance of the two models. For this

reason, the inclusion of 100 years is more desirable because it increases confidence in the results while providing a paradigm of how models should operate.

For precipitation, wind stress, and upper ocean variables 100 years of data is not available. 60 years of precipitation and wind stress values from NCEP-NCAR Reanalysis I from January 1948 to December 2007 provide a general framework for describing the shortcomings of modern climate models. There is evidence challenging the validity of the NCEP-NCAR Reanalysis data particularly with precipitation (Trenberth and Guillemot 1998). For our purposes the limitations of NCEP-NCAR are worth mentioning so as to explain the usefulness of this dataset in this study. Even when model estimates are biased, the interannual variability tends to be correlated with independent observations (Kistler et al. 2001). Other datasets available have biases also, for example, ECMWF Re-analysis -40 (ERA-40) has known issues with tropical precipitation (Uppula 2005). Furthermore, most datasets which correct issues with NCEP-NCAR Reanalysis are for shorter periods than 60 years. Because of the interdecadal changes in ENSO mentioned earlier, the longer dataset is preferred where possible.

At the time of this study, 30 years of GODAS data allow comparison of upper ocean conditions that would otherwise be unavailable. Because GODAS uses the ocean model Modular Ocean Mode (MOM), an ocean model physically similar to POP, to assimilate observations, the model control run for CFS is used to validate the results.

In order to make a fair comparison between datasets with different trends and because several of the data analysis methods used assume the data to be stationary, detrending of datasets was preformed. The linear trend of each data set is calculated from only the months used for data analysis. The trends were calculated and removed for all variables used in this study. Fig. 2.1 shows the trend for equatorial Pacific SSTs

in degrees Celsius per year. For the 100 years used, ERSST has a uniform warming trend throughout the Pacific. CAM-HYCOM shows an El Niño like warming whereas CAM-POP shows no significant trend over the 200 years of model integration.

2.2 Derived Variables

Two calculations were performed on native data fields in order to conduct this study: calculation of the thermocline depth and the interpolation of ocean model HYCOM native grid to physical coordinate gird. The thermocline depth is a 2-dimensional field derived from the depth of the 20° C isotherm. Linear interpolation was used to measure the temperature depth between levels. By definition this is not the true thermocline depth, however, in the equatorial Pacific it is a good approximation especially for twentieth century control runs (Yang and Wang 2009). Unlike the other datasets used, HYCOM model output is produced in native coordinates and was converted to physical z-coordinates. This is an important consideration especially for the vertical component of the current.

2.3 Analysis Methods

Initial work undertaken in this study follows the work in Misra et al. (2008) which provides an examination of modeled ENSO characteristics. Analysis methods presented in this study focus largely the Niño 3 index derived by taking area averaged temperature over the Niño 3 region (Fig. 1.2). The Niño 3 index was chosen over the various other regions because it has been shown to be well correlated with the SOI and because the models and datasets used in this study have a large amount of variance in that region. Because of the differences between ENSO variability across the models used, this index is often normalized to produce comparable results. The

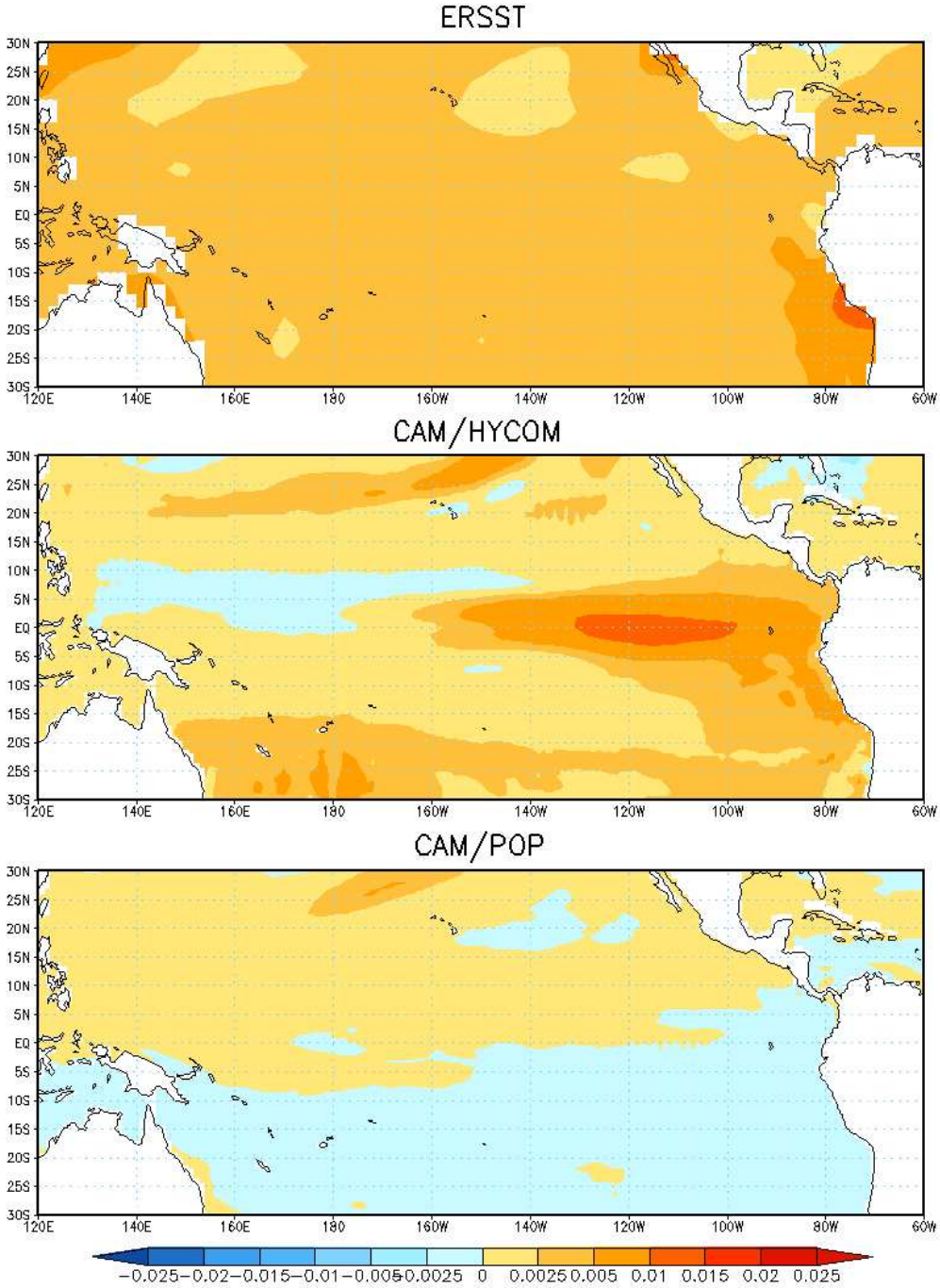

Figure 2.1: SST trends of the tropical Pacific in degrees Celsius per year for a) ERSST, b) CAM-HYCOM, and c) CAM-POP.

normalized index is the anomalous Niño 3 SST divided by the standard deviation of the index.

For this study three advanced signal processing methods or data analysis tools were used: principal component analysis, spectral analysis, and ensemble empirical mode decomposition (EEMD). The first two have attained popularity in the scientific community and will be briefly described here. The new lesser-known signal processing method, EEMD, will be discussed in more detail.

Principal component analysis (PCA) is a mathematical technique which effectively reduces the dimensionality of a data set consisting of a large number of interrelated variables (Jolliffe 2002). The result is a set of orthogonal data sets called empirical orthogonal functions (EOF) with only a few EOFs containing the majority of the data needed to reproduce the original data set. In instances where the original data contained a physical signal, the resulting EOFs can usually be interpreted physically. For the study of ENSO, PCA is commonly used to find the spatial extent of SST anomalies for a typical ENSO event.

The Fourier transform of a time series provides a spectral space examination of the data. There is, however, uncertainty when using a discrete time series. Many methods exist to extract a higher level of certainty from a limited amount of data. In this study we have chosen to use the maximum entropy method (MEM) (Penland et al. 1991) to extract the most probable spectrum from the limited amount of data available. The advantage of MEM is that confidence limits are not needed examine the resulting spectrum.

EEMD is a data driven analysis method which involves the decomposition of a time series into intrinsic mode functions (IMF). Each IMF contains a separate physical mode, for example a diurnal cycle or an annual cycle. The first step in generating each IMF is done by creating an upper and lower enveloping function for the data. When

the average of these two envelopes is removed, the result is an IMF which contains the highest frequency signal of the data. The process is repeated on the remaining data until no more IMFs can be generated.

Signal intermittence in a time series can lead to what is known as "mode mixing". Mode mixing, as the name suggests, is the presence of multiple modes within a single IMF and occurs because the enveloping functions fit the data maxima. If a particular mode is absent for part of the time series then the enveloping process will capture another mode outputting an IMF with multiple modes. Adding white noise to the intermittent mode reduces the mode mixing substantially. By repeating this process with multiple ensemble members, each with a different sample of random noise added, IMFs produced do not have any noise because of the expectation of white noise is zero (Wu and Huang 2009).

In this study, EEMD was done on the Niño 3 SST time series. A Gaussian distributed white noise with standard deviation of 0.2 was added to each of 100 ensemble members to produce the IMFs. After this initial decomposition, there was still mode mixing between the two IMFs of interest: the biennial and ENSO modes. The first two IMFS (monthly weather "noise" and annual cycle) were removed from the original time series. The remaining data was processed with a single ensemble member with no noise added producing the true IMF for Biennial and ENSO oscillations.

Beyond the three analysis methods listed above, a detailed analysis of the SST anomaly equation was preformed. Equation 2.1 is the time tendency of the anomalous temperature from (Kang et al. 2001). Calculating this equation for the upper 50 meters of the ocean produces a SST anomaly tendency equation. Following Misra et al. (2008), the regression of Niño 3 SST tendency on each advection term in the SST tendency equation were plotted to diagnose the importance of each advective

term on ENSO events.

$$\frac{\partial T'}{\partial t} = -\bar{u}\frac{\partial T'}{\partial x} - u'\frac{\partial T}{\partial x} - \bar{v}\frac{\partial T'}{\partial y} - v'\frac{\partial T}{\partial y} - \bar{w}\frac{\partial T'}{\partial z} - w'\frac{\partial T}{\partial z} - Q' \tag{2.1}$$

Equation 2.1: the temperature anomaly tendency equation where T is temperature; u, v, and w are zonal, meridional and vertical velocity; and Q' is the anomalous heat source/sink term. Prime terms indicate anomalies; over-line terms indicate seasonal means.

Other features of ENSO were examined using a variety of methods. The standard deviation of monthly Niño 3 SST shows the period of strongest ENSO activity. Autocorrelation of the Niño 3 SST at various time-lags provides a measure of the decorrelation time, the relative length of an ENSO event. Linear regression across the Equatorial Pacific with a Niño index gives perspective on spatial patterns related to changes in that index. Time-lag regressions were also preformed for 3-D ocean features. The Student's t-test was used to find the significant regression coefficients. Both correlation and regression involve the product of two variables; to calculated the time-lagged quantities, the product of variable x at time t and variable y at time $t+$ lag is used.

CHAPTER 3

RESULTS

3.1 Return Period and Duration of ENSO

Fig. 3.1 shows the resulting Niño 3 SST spectra for ERSST, CAM-HYCOM, and CAM-POP using MEM. The ERSST spectrum of SST in this region contains a broad peek at roughly 4.5 years spanning from 2 to 7 years. This illustrates, very clearly, the irregular return period of ENSO. A much weaker, but nonetheless equally broad, peak is seen in CAM-HYCOM centered around 4 years. CAM-POP has a slightly stronger, narrower peek compared to CAM-HYCOM centered near 4.5 years. CAM-POP exhibits strong variance in the Niño 3 region on a two-year time scale. As has been shown in other studies, (Guilyiardi 2006) this biennial oscillation is a prominent problem with the coupled model, CAM-POP. Yu. et al. (2007) suggests this is related to the Indian monsoon and changes to the convection scheme in CCSM3.5 corrected this issue. Even so, CAM-HYCOM does not show any erroneous biennial oscillation; this will be important when analyzing later results.

Use of the autocorrelation as done in Joseph and Nigam (2006) provides a quantifiable estimate for the duration of a typical ENSO event. As a benchmark, e-folding time scale is used to measure the decorrelation time for an event interval; this provides a standard by which to measure the duration of ENSO events. The autocorrelation

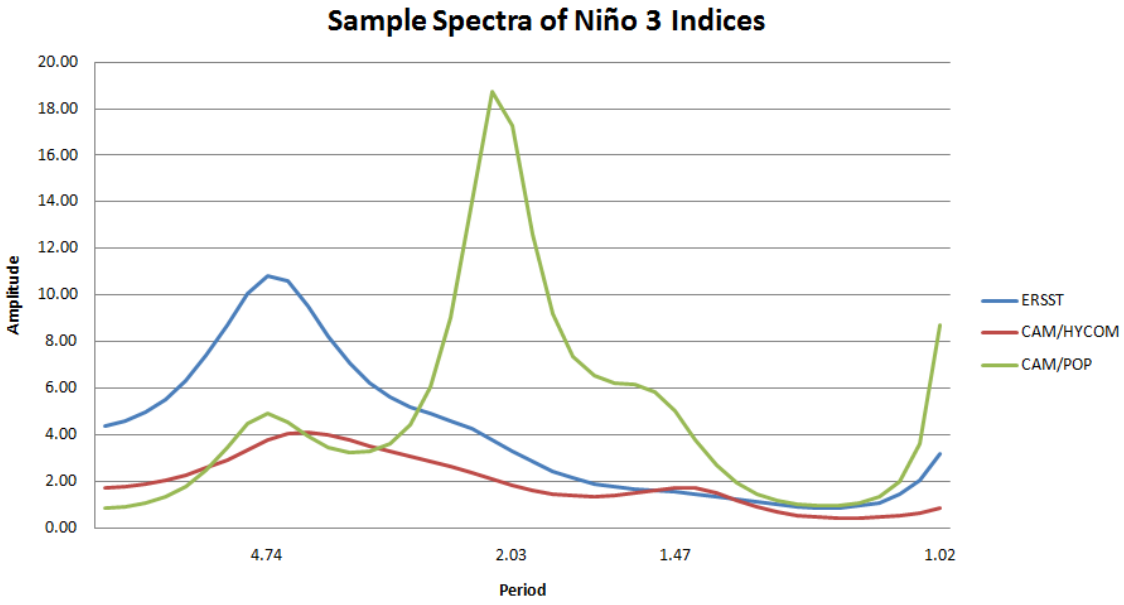

Figure 3.1: Sample Spectra of Niño 3 SST generated using the Maximum Entropy Method for ERSST (blue), CAM-HYCOM (red), CAM-POP (green)

of the Niño 3.4 SST index (Fig. 3.2) reveals that the time scale for modeled ENSO events is shorter in length than shown in ERSSTv3. Observations (ERSST, blue) have an interval of around 12 months for an average event. Autocorrelation at 12 months for CAM-POP shows negative relationship, a result of the strong biennial cycle. The negative autocorrelation at 12 months for CAM-POP shows that the opposite phase of variability is occurring the following year (ENSO events occur at regular intervals) as a result of the strong biennial cycle in CAM-POP. CAM-HYCOM has improved correlation compared to CAM-POP and possibly improved the ENSO event duration slightly. Autocorrelation of CAM-HYCOM, like many models, shows a stronger annual cycle compared to observations. This is evidenced by the more pronounced local maxima at 12 month lag, seen in CAM-HYCOM compared to ERSST.

3.2 Seasonal Phase-Locking of ENSO

Reproduction of seasonal phase locking in coupled models is important for seasonal forecasting and a good test of ENSO fidelity in models. Observations show that ENSO variability usually peaks in boreal winter. ENSO variability tends to fall off in the spring and remain low up until early fall Rasmusson and Carpenter (1982). There are recorded events which do not follow this pattern but for the most part, this is a striking characteristic of ENSO. In models with a proper ENSO simulation, we should see a seasonal cycle of variance similar to this.

For ERSST (Fig. 3.3), the seasonal variance peaks in November-December and quickly drops to a minimum by March-April. What is seen in the two models is that the coupled CAM-HYCOM model does not have a phase locking characteristic whereas CAM-POP does. Fig. 3.3 shows the standard deviation of the Niño 3 SST for ERSST, CAM-HYCOM, and CAM-POP. A loose reproduction of ERSST's pattern

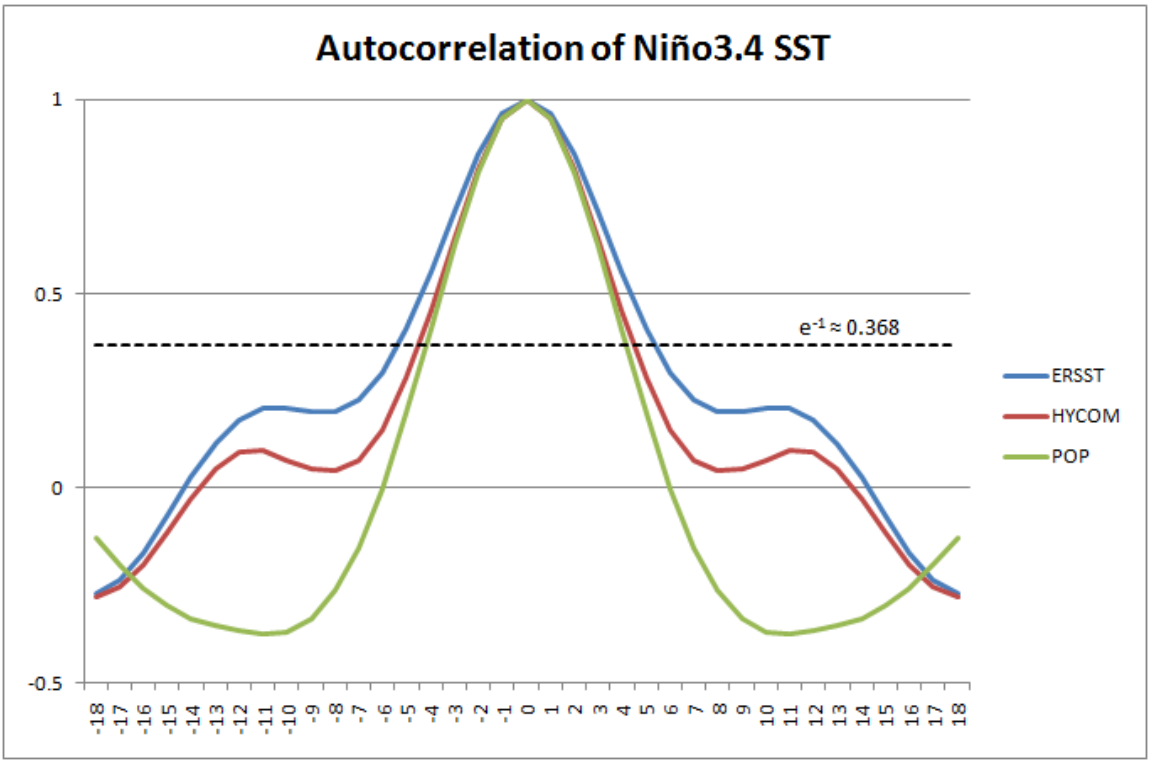

Figure 3.2: Autocorrelation of Niño 3 SST ERSTT (blue), CAM-HYCOM (red), CAM-POP (green). The dashed line is drawn at e^{-1} to estimate the duration of the event during one phase of ENSO.

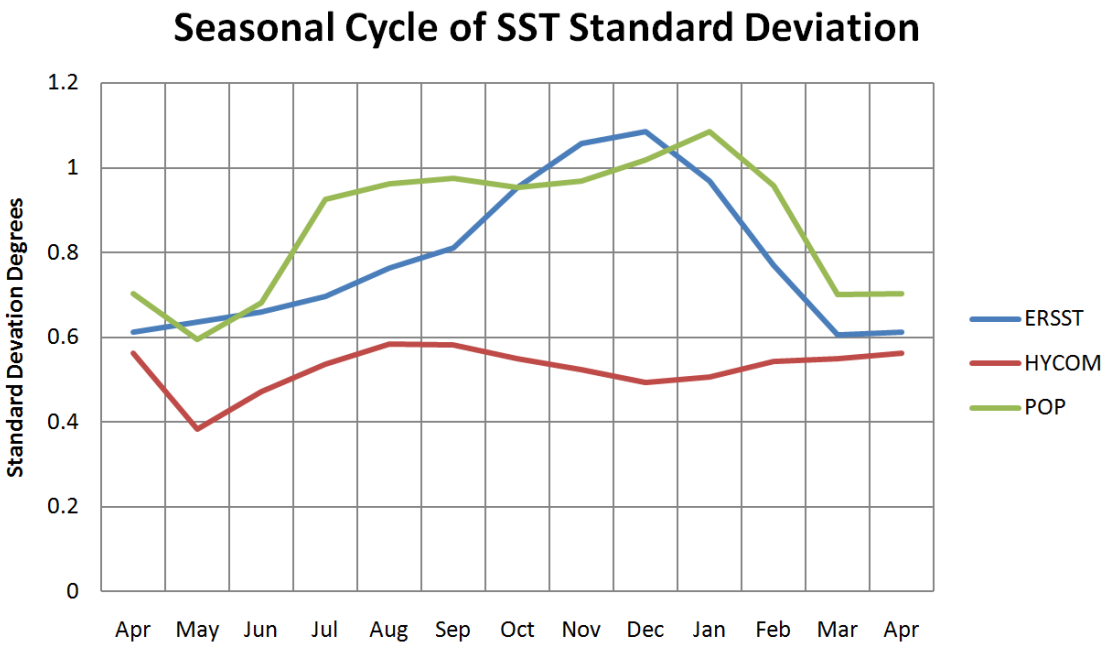

Figure 3.3: Seasonal cycle of Standard Deviation of SST in Niño 3 Region for ERSST (blue), CAM-HYCOM (red), CAM-POP (green).

is seen in CAM-POP. In CAM-HYCOM, the standard deviation is nearly flat. This would suggest that there is no preferential peak for an ENSO phase in CAM-HYCOM but is also an artifact of the low variance on ENSO time scales as seen in Fig. 3.1. The next section will expand on the poor seasonal phase-locking seen in CAM-HYCOM and CAM-POP.

3.3 Mean Thermocline Depth and Seasonal Cycle of SST

The average thermocline depth is an important feature of the Equatorial Pacific Ocean. Proper simulation of thermocline is necessary for the correct Eastern Pacific SST response in ENSO models. Fig. 3.4 shows GODAS mean state in blue; the

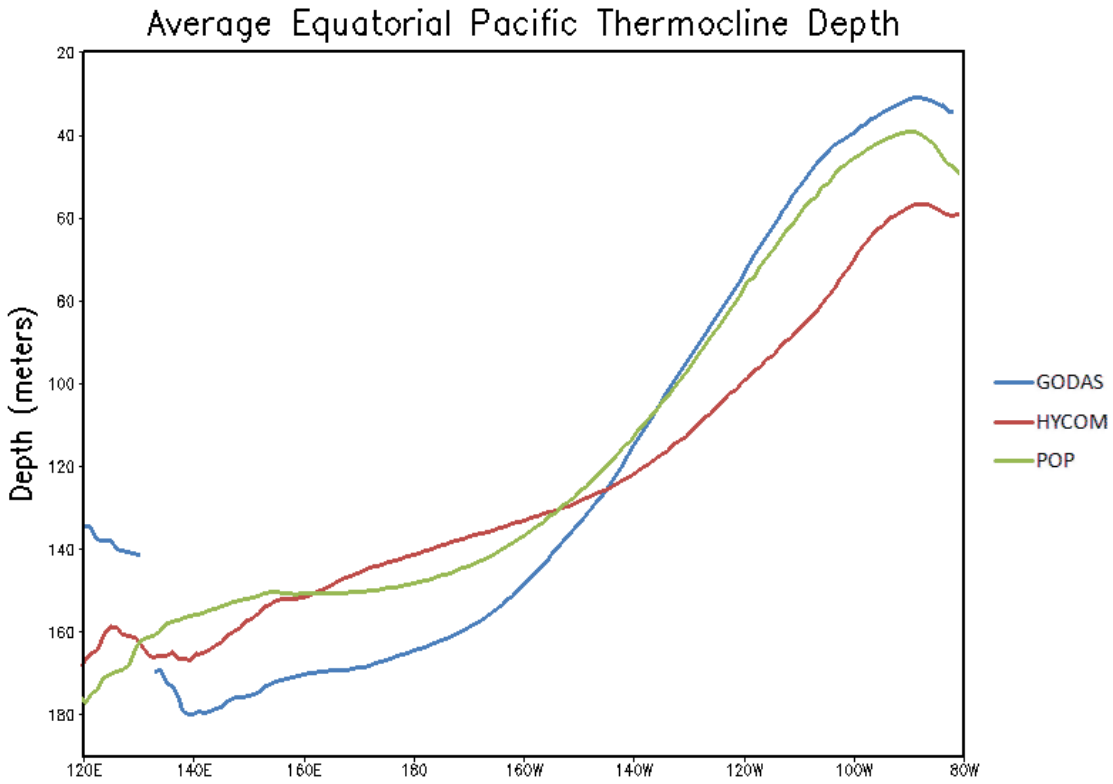

Figure 3.4: Average Equatorial Pacific Thermocline Depth for GODAS (blue), CAM-HYCOM (red), CAM-POP (green).

average thermocline depth is near the surface in the east and deep in the west. In the Eastern Pacific, CAM-POP does well at simulating the observed mean state whereas CAM-HYCOM has a thermocline that is too deep. In the west, both models fail to deepen the thermocline to the extent found in observations. It should be noted, however, that the correct simulation of the Eastern Pacific thermocline is central to producing accurate SSTs in this region. The low Niño 3 SST variance in CAM-HYCOM can be attributed to the poor thermocline tilt.

The majority of tropical Pacific variability takes place to the east of the International Date Line. The left panel in Fig. 3.5 shows the climatological seasonal cycle of SST (ERSST). Temperatures in the east peak in early spring thus decreasing the

zonal temperature gradient. The reduced gradient lowers zonal wind stress (decreased upwelling) leading to the observed westward progression of warm water from boreal winter to spring. CAM-HYCOM makes little improvement over CAM-POP in this respect: both models lack a robust westward migration pattern. Furthermore, the warming does not emanate from the coast as seen in ERSST. CAM-HYCOM does ameliorate the dipole effect seen in the central Pacific in CAM-POP but introduces more errors in the far West Equatorial Pacific.

In this respect the differences in OGCMs have not substantially altered the simulation of seasonal cycle. This would suggest that the seasonal cycle is not the cause of the differences seen in the ENSO periodicity. To test this theory, we must examine the dominant air-sea interactions governing the observed seasonal cycle.

Gill's seasonal cycle explains the major mechanism for the seasonal cycle in the Eastern Equatorial Pacific Guilyiardi (2006). The black line in Fig. 3.6 shows the three phases of the relationship between upwelling and SST in the Equatorial Pacific. First, during March-May (MAM) the SST in the Eastern Tropical Pacific is the greatest as the wind stress relaxes. Second, during the boreal summer and autumn months (JJA) and (SON) SSTs decrease. Third, during boreal winter (DJF) zonal wind stress is at a maximum. Li and Philander (1996) shows that the seasonal cycle is a result of the climatic conditions in the Eastern Tropical Pacific. GODAS maintains the seasonal cycle of SST shown in both the NCEP-NCAR Reanalysis and in Guilyiardi (2006) but the magnitude of wind stress is systematically stronger. Both models (CAM-HYCOM and CAM-POP) fail to capture the spring relaxation of zonal wind stress which suggests the apparent phase locking seen in CAM-POP is caused by a different mechanism than that in the real climate system; most likely, the phase locking in CAM-POP is a result of the strong biennial oscillation as shown in Fig. 3.1. The relatively higher SSTs seen in CAM-HYCOM compared to CAM-POP reflect the

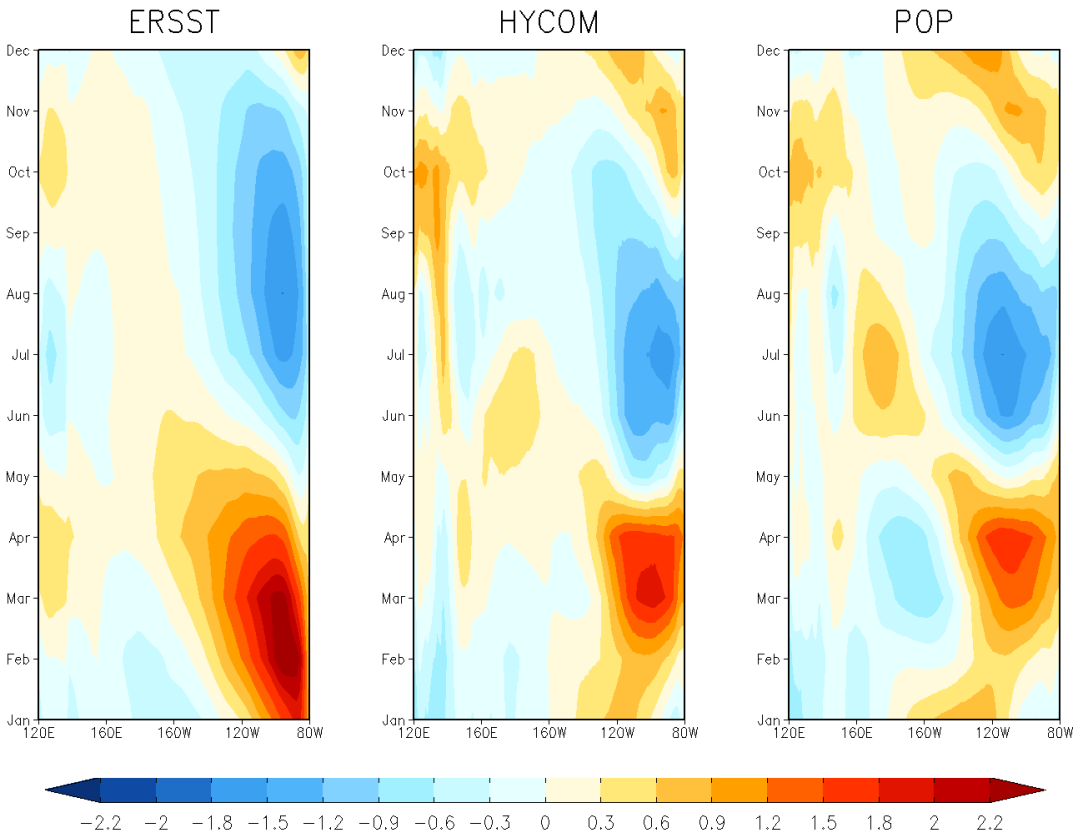

Figure 3.5: The Climatological Annual Cycle of SST in Celsius in the Equatorial Pacific for a) GODAS b) CAM-HYCOM c) CAM-POP

differences in thermocline depth; the relative decrease in wind stress follows from the decreased temperature gradient along the Equatorial Pacific.

3.4 Spatial Extent of Eastern Pacific SST Interannual Modes

The first EOF of the Tropical Pacific SSTs can be physically interpreted as ENSO variability. Fig. 3.7 shows first EOF of SST for ERSST, CAM-HYCOM, and CAM-POP over the domain 20S-20N, 120E-60W. The pattern of SST for ERSST shows the maximum variance located within 5^oS-5^oN extending from the South American coast stopping at the date line. CAM-HYCOM has a similar pattern but with much weaker signal (as expected from spectral analysis above). CAM-HYCOM also displaces the maximum variance away from shore. Typical of many coupled models, CAM-POP has a stronger, more zonal pattern extending far past the date line. CAM-HYCOM can be seen as an improvement over CAM-POP for the shape of the ENSO signal.

Regression of Niño 3 index on tropical Pacific SSTs is another common method used to plot the spatial extent of ENSO variance. In Fig. 3.8 the observed "horse-shoe" pattern is lacking in the CAM-HYCOM and CAM-POP versions of ENSO. Both CAM-HYCOM and CAM-POP have a zonal pattern with a north-south dipole across the Pacific as compared to ERSST. Here, CAM-HYCOM exhibits a stronger-than-observed variance off the coast of Peru – a striking difference from CAM-POP which puts core of variance further west, away from the coast. Because this analysis contains biennial variance in addition to ENSO variance, the differences between CAM-HYCOM and CAM-POP here are indicative of the reasons for the absence of a strong biennial oscillation in CAM-HYCOM. For comparison, Fig. 3.9 shows the same regression as Fig. 3.8 but for ERSST, GODAS, and NCEP-NCAR. These three

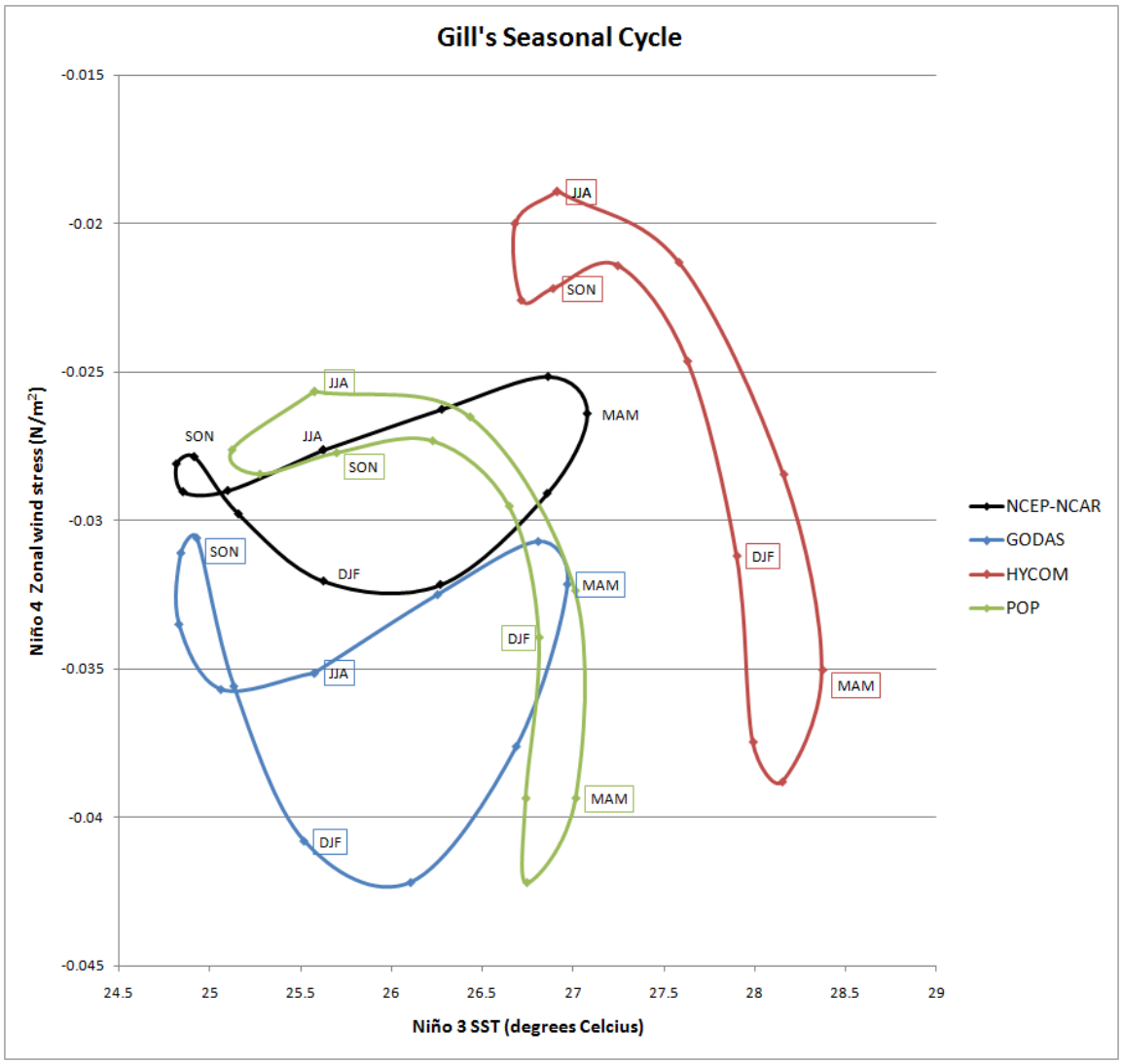

Figure 3.6: Seasonal Cycle of Niño 3 SST against Niño 4 Zonal Wind Stress for NCEP-NCAR Reanalysis (black), GODAS (blue), CAM-HYCOM (red), CAM-POP (green).

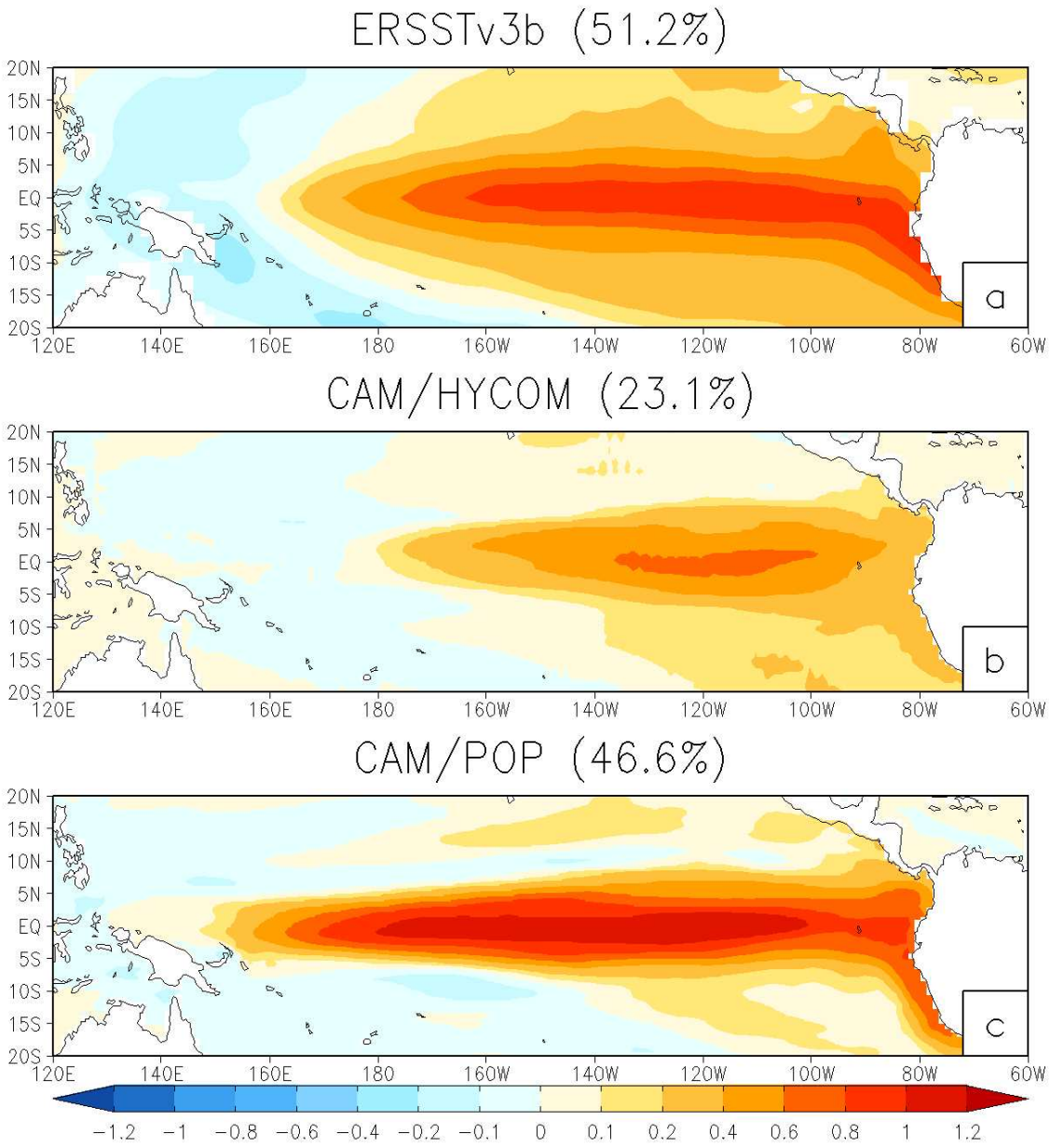

Figure 3.7: First Empirical Orthogonal Function for Equatorial Pacific SSTs for a) ERSST, b) CAM-HYCOM, and c) CAM-POP (precentages show variance explained)

panels look similar because the SSTs assimilated into GODAS and NCAP-NCAR are principally identical to ERSST. Regression of the Niño 3 Index on SST also provides verification that the EOF plotted in Fig. 3.7 has a physical interpretation. For ERSST, the differences between Fig. 3.7 3.8 are likely the cause of analysis method used and the results can be viewed as consistent. For CAM-HYCOM, the high variance near the coast of Peru represents a departure from the first EOF. As such, we can assume the coast upwelling is important in the variance of the Niño 3 region where as in CAM-POP it is not. Lastly, the first EOF of CAM-POP is probably highly correlated to the biennial oscillation in addition to or in place of ENSO.

As we have already seen, the Niño 3 Index for CAM-POP contains a large biennial component. To analyze the effects of this component, EEMD of the Niño 3 SST was used to extract the biennial mode (IMF1) and the ENSO mode (IMF2) from each time series. Fig. 3.10 shows a 6-year sample of IMF 1 and 2 from near the beginning of the time series for ERSST, CAM-HYCOM, and CAM-POP. This illustrates the differences in magnitude of the modes for each dataset. As expected, the magnitude of IMF1 is relatively weaker than IMF2 for ERSST and CAM-HYCOM. For CAM-POP, IMF2 is weaker than IMF1. Thus, the biennial oscillation is a central component of Niño 3 Index in CAM-POP. Fig. 3.11 gives the regression of IMF1 (biennial oscillation) on SSTs. Note the similarities between the IMF1 regression (Fig. 3.11) and Fig. 3.8 contrasting the EOF analysis (Fig. 3.7). The negative correlation seen in the northern tropical Pacific is a significant feature of the biennial oscillation in CAM-HYCOM and CAM-POP. In CAM-HYCOM, the high variance in the coastal Peruvian region also appears to be biennial.

Fig. 3.12 is the regression of IMF2 on the Equatorial Pacific SSTs for ERSST, CAM-HYCOM, and CAM-POP. This might be considered the closest representation of 'true' ENSO variability available. Here, the model variance in the Northern Equa-

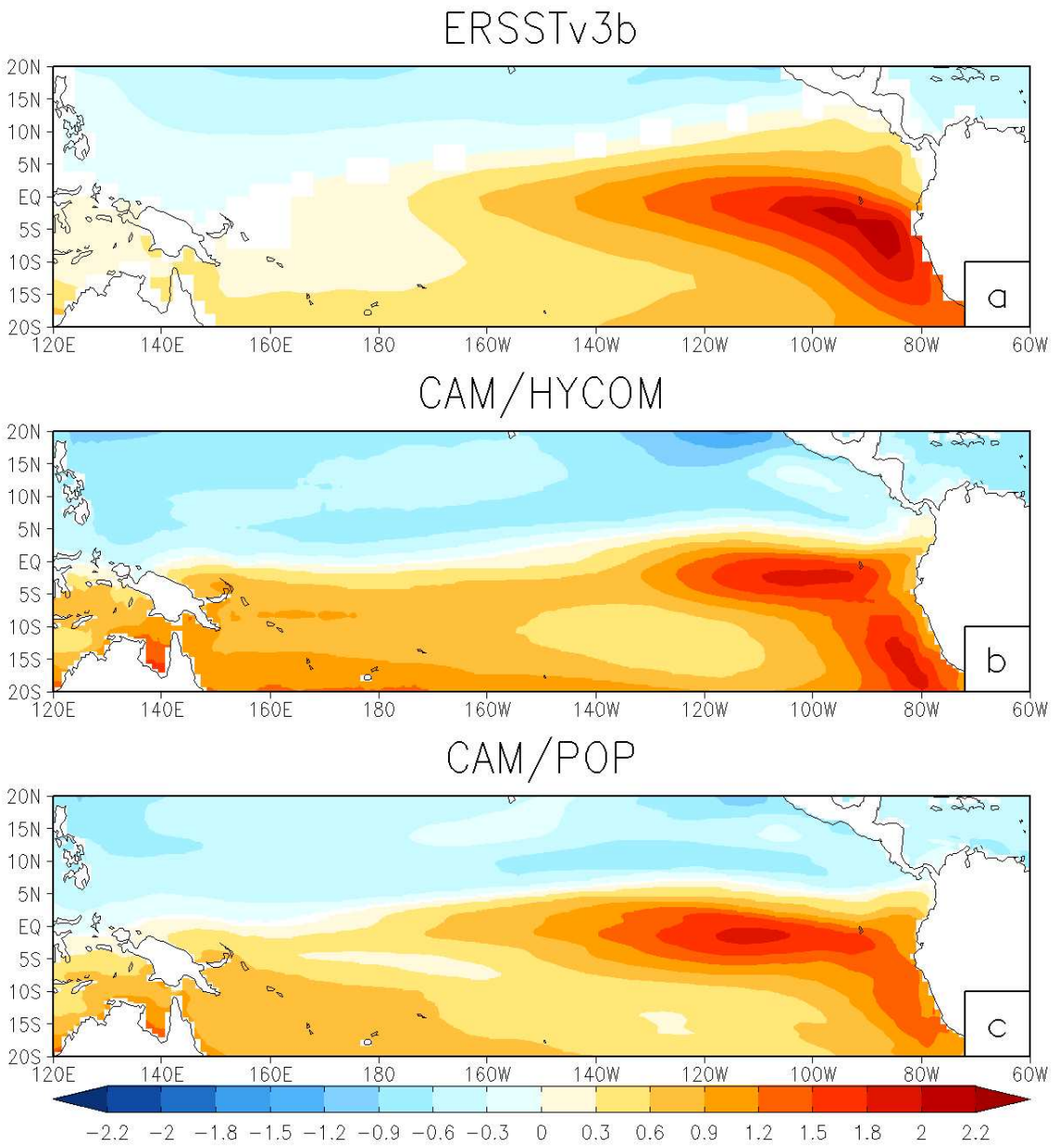

Figure 3.8: Regression of Niño 3 Index on SST in Celsius normalized by Niño 3 SST for a) ERSST, b) CAM-HYCOM, and c) CAM-POP. Only values significant at 95% confidence limit are plotted.

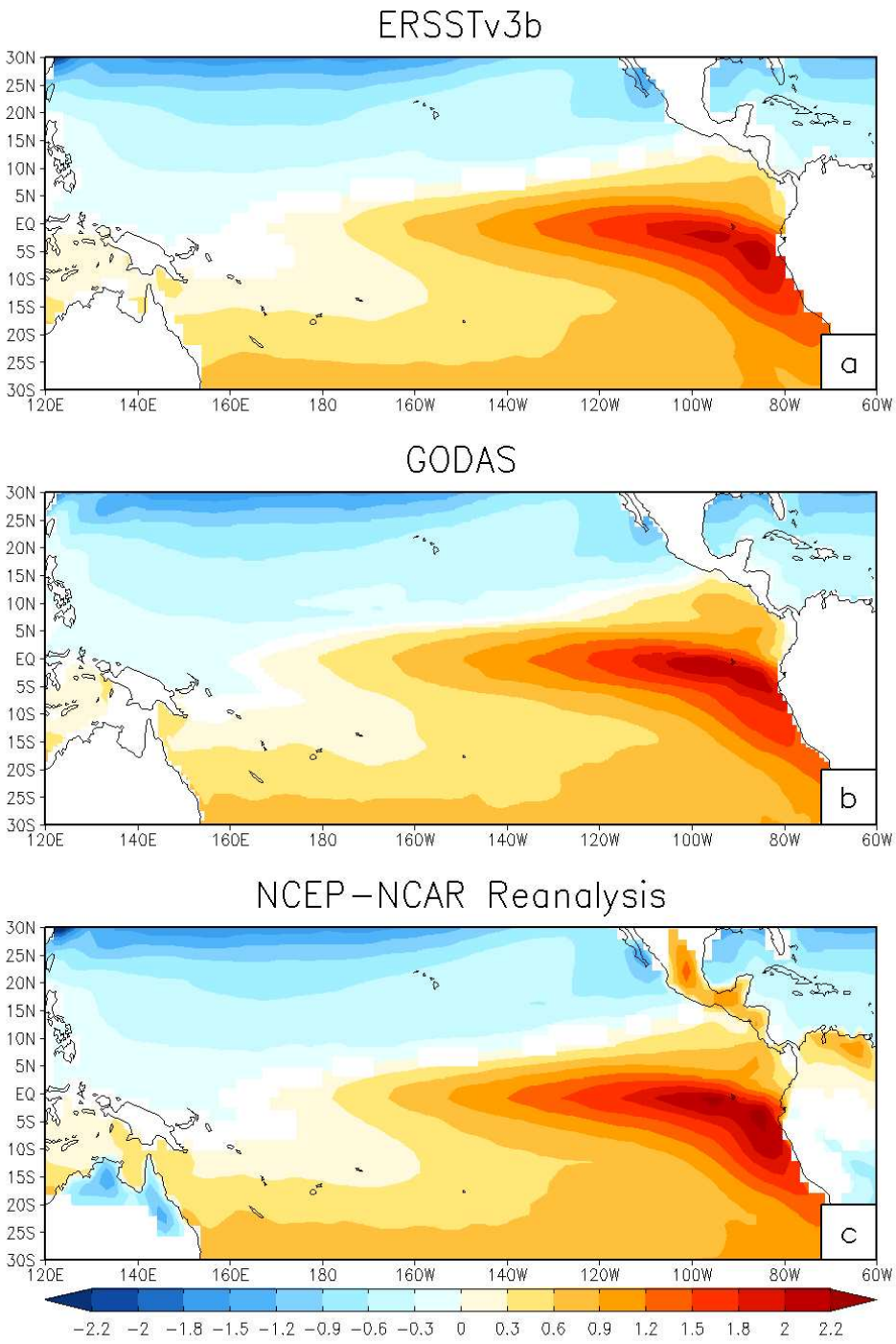

Figure 3.9: Regression of Niño 3 Index on SST in Celsius normalized by Niño 3 SST for a) ERSST, b) GODAS, and c) NCEP-NCAR. Only values significant at 95% confidence limit are plotted.

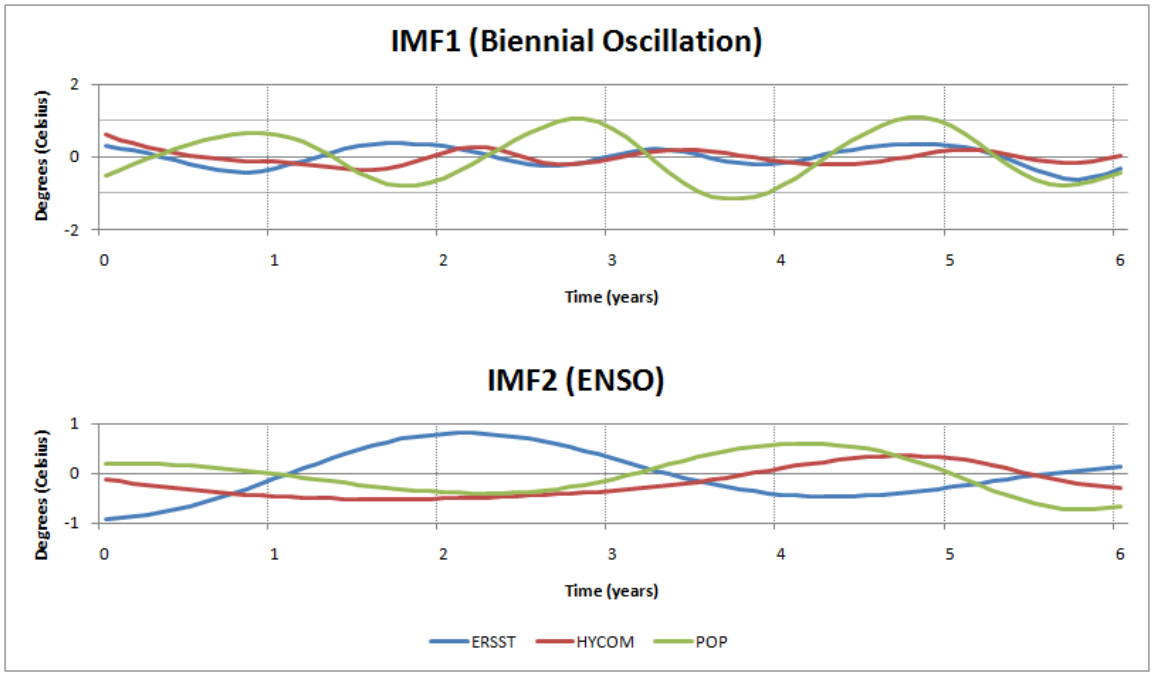

Figure 3.10: 6-year sample of IMF 1 and 2 for a) ERSST, b) CAM-HYCOM, and c) CAM-POP.

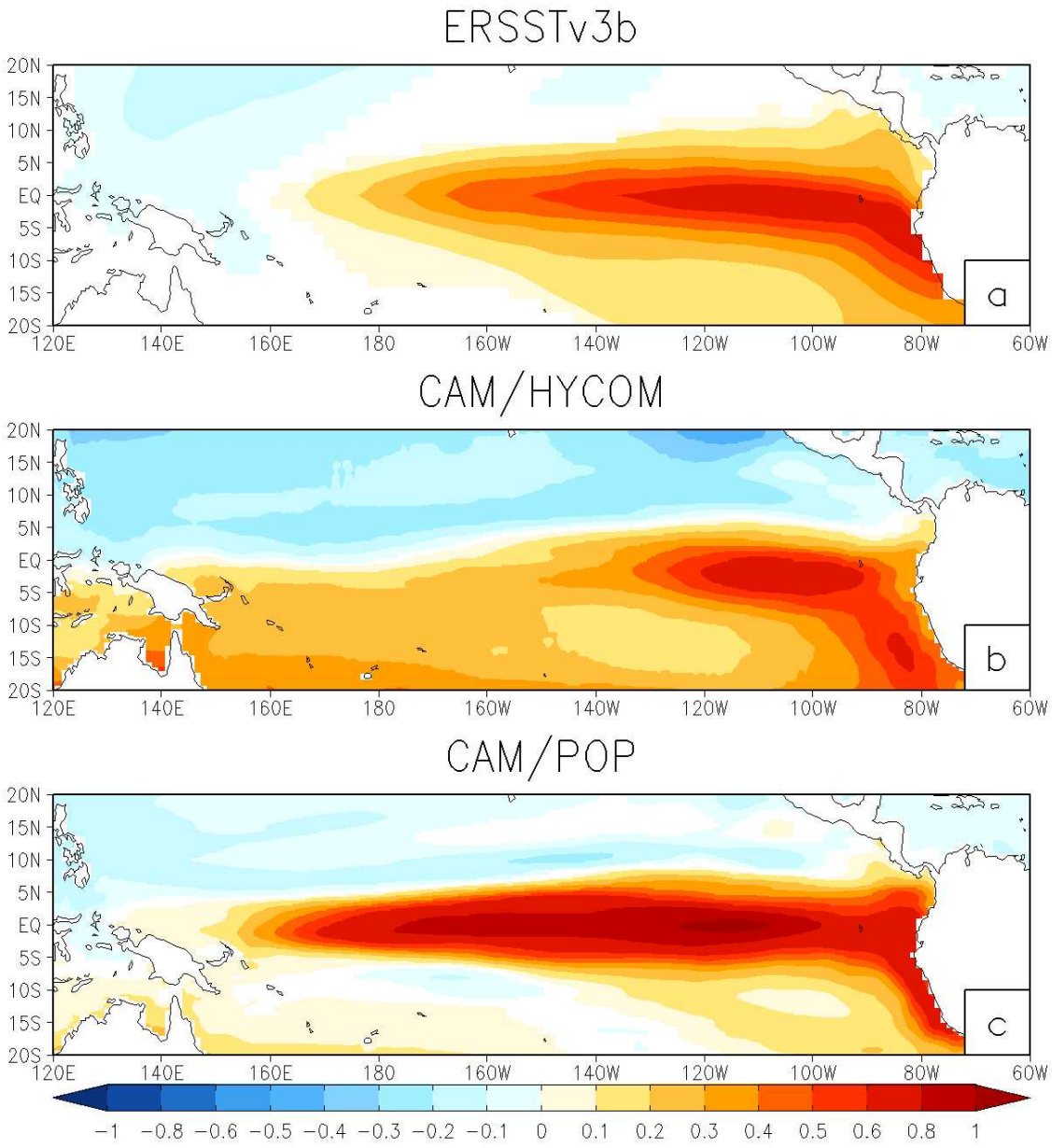

Figure 3.11: Regression of IMF1 (biennial oscillation) on SST in Celsius normalized by IMF1 for a) ERSST, b) CAM-HYCOM, and c) CAM-POP. Only values significant at 90% confidence limit are plotted.

torial Pacific is mostly positive or below the 90% significance limit. It is also apparent that IMF2 more closely resembles the first EOF (Fig. 3.7) than the regression shown in Fig. 3.8. For CAM-HYCOM, variance on ENSO time-scales is located east of the date line with a maximum in the Niño 3 region. ENSO time-scale variance in CAM-POP extends beyond the date line with a maximum in the Niño 3.4 region. The horseshoe pattern emerges in the regression of IMF2 on SSTs for CAM-POP but does not have the robustness seen in ERSST. It is likely that CAM-HYCOM also has this trait but, since ENSO variability is weaker in CAM-HYCOM, the relationship is not significant. The remainder of analyses will not use IMF2 unless otherwise noted.

3.5 Upper Ocean Response/Feedback to Niño 3 SST

Diagnosing the ocean's role in the air-sea interactions responsible for ENSO requires an examination of the thermocline depth. EOF analysis of the observed thermocline depth preformed in Clarke et al. (2007) uncovered two primary modes of the thermocline variance. The first mode constitutes about 50% of the variance and is dubbed the 'tilt mode' for the zonal tilting of the thermocline associated with this phase; this mode is also highly correlated with the Niño 3 Index. The second mode is the discharge and recharge mode which is correlated to the time derivative of the Niño 3 Index. Together, these two modes are essential for the evolution of ENSO. Panel 'a' of Fig. 3.13, the regression of Niño 3 SST on thermocline depth, demonstrates the tilt mode described by Clarke et al. (2007) as seen in GODAS. The see-sawing of the thermocline pivots at around 160^{o} W. Panel 'b' and 'c' show the same regression for CAM-HYCOM and CAM-POP respectively. For CAM-HYCOM, the pivot point appears to the east and there is a spurious correlation in the far West Pacific.

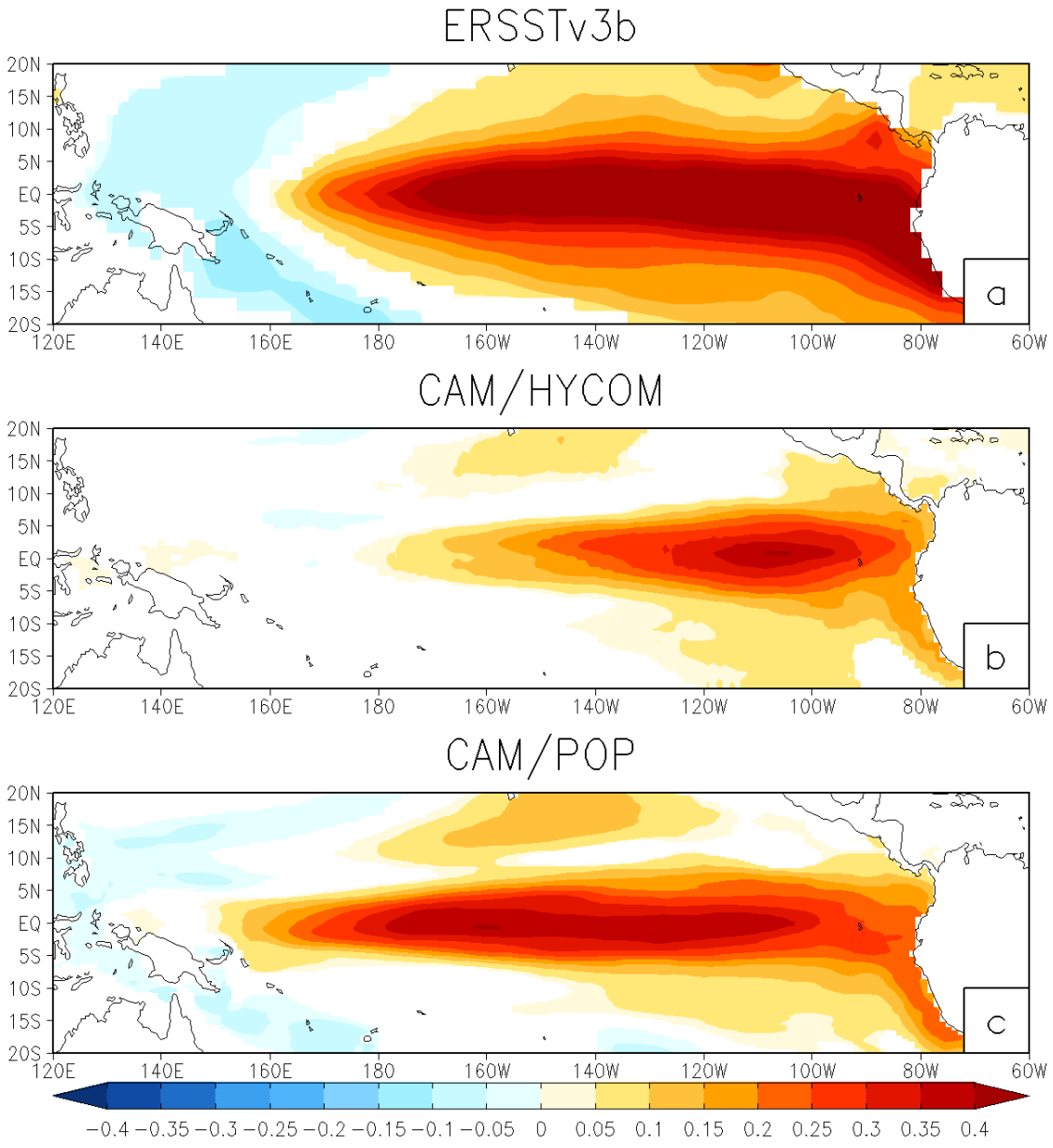

Figure 3.12: Regression of IMF2 (ENSO) on SST in Celsius normalized by IMF2 for a) ERSST, b) CAM-HYCOM, and c) CAM-POP. Only values significant at 90% confidence limit are plotted.

CAM-POP reproduces the SST-thermocline relationship better than CAM-HYCOM but still places the pivot point east of 160° W

Further investigation into the model behavior shows that the thermocline tilting on ENSO timescales is more characteristic of the observed tilt. Panel 'd' and 'e' show the regression of IMF2 on thermocline depth for CAM-HYCOM (d) and CAM-POP (e). The unusual positive values in the west for CAM-HYCOM, seen in panel 'b', are not present on ENSO timescales. Additionally, the pivot point is now further west. This suggests that recharge-discharge is present in both models. In order to confirm this, the warm water volume (WWV) recharge/discharge should correlate well with the time derivative of Niño 3 SST. This can be seen in Fig. 3.14, the regression of Niño 3 SST tendency on thermocline depth. Both models have positive anomalies of thermocline depth along the equator which matches GODAS. GODAS also exhibits a symmetric pattern about the equator with larger variance in the central Pacific. CAM-HYCOM and CAM-POP have asymmetric patterns with larger variance in the northern hemisphere.

In addition to the state of the upper ocean in relation to Eastern Equatorial Pacific SST and SST tendency, the time evolution of the upper ocean is important. Fig. 3.15 show the Lag-regression of Niño 3 Index on thermocline depth. At zero lag, GODAS shows the tilting mode as shown in Fig. 3.13. At 8-month lag, GODAS shows the recharge phase.

This can be seen as the migration of the equatorial Kelvin waves emanating from the Central Pacific to East Pacific after an anomalous wind stress occurs in the Central Pacific as explained by the Delayed Oscillator Theory (DOT). At 12-months lag, the Western Pacific has an anomalous positive thermocline correlation. Noteworthy is the absence of any correlation in the east at 12-month lag; this is because of the irregularity of ENSO return period. In CAM-HYCOM (ignoring the spurious

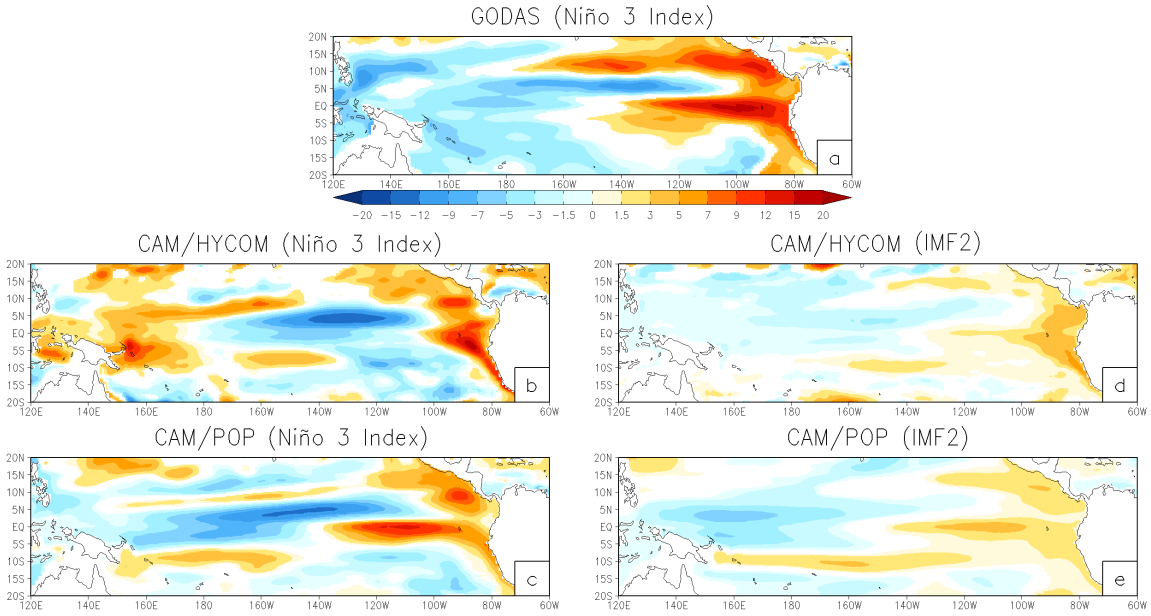

Figure 3.13: Regression of Niño Index on Thermocline Depth normalized by Niño 3 SST for a) ERSST, b) CAM-HYCOM, and c) CAM-POP; Regression of IMF2 (ENSO) on Thermocline Depth normalized by IMF2 for d) CAM-HYCOM, and e) CAM-POP. Values given in meters significant at 90% confidence limit.

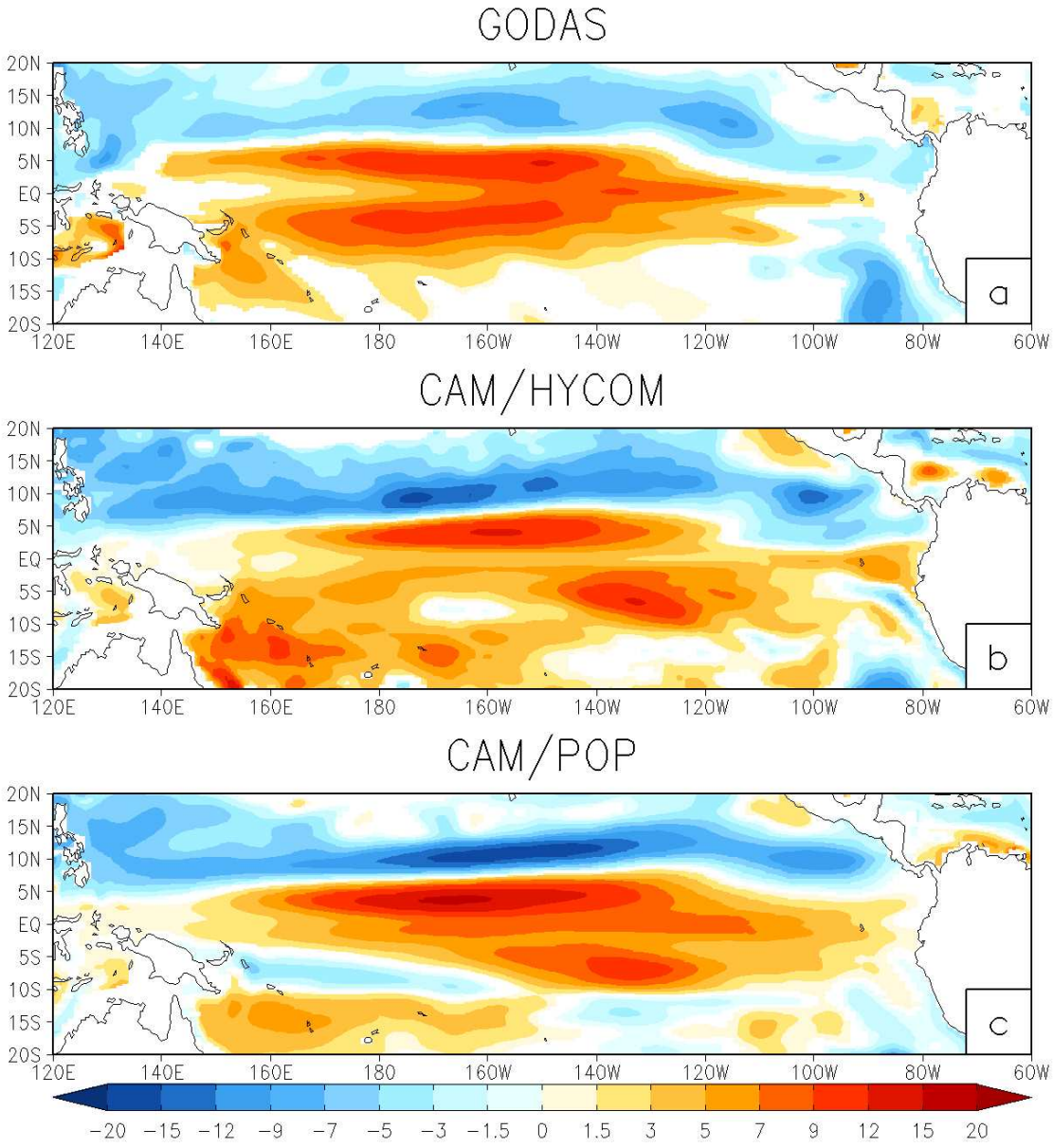

Figure 3.14: Regression of Niño 3 SST Tendency on Thermocline Depth normalized by Niño 3 SST Tendency for a) ERSST, b) CAM-HYCOM, and c) CAM-POP. Values given in meters significant at 90% confidence limit.

correlations in the far west) the migration of equatorial Kelvin waves takes place over a 6-month period indicating the shorter interval between events. CAM-POP also speeds up the migration of equatorial Kelvin waves but the values show a strong regression to the previous inverse because of the biennial cycle in that model. Thus, the primary ocean oscillation in CAM-POP (the biennial oscillation) can be explained in terms of the DOT. The tendency in CAM-POP for the thermocline depth in the central Pacific to deepen more than the east is likely because of the warm events occurring more in the central Pacific than is observed.

3.6 Atmospheric Response/Feedback to Niño 3 SST

Both coupled models examined contain the same atmospheric model, however, the air-sea feedbacks within the coupled system could cause the atmospheric component of the models to vary. Atmospheric components of ENSO inspected include the precipitation, a proxy for the Walker and Hadley circulation modulation, zonal wind stress, an indicator of the positive feedback mechanism inducing ENSO events, and 200 hPa heights over North America, a sample of the associated teleconnections of ENSO.

First, we examine the precipitation pattern associated with ENSO. Fig. 3.16 shows the Regression of Niño 3 Index on precipitation. For NCEP/NCAR the modulation of the walker circulation is apparent; in the normally dry Eastern Pacific there is a significant positive anomaly of precipitation whereas the maritime convenient is negatively correlated to East Pacific SSTs. CAM-HYCOM and CAM-POP have a zonal positive correlation with Eastern Pacific SSTs. The strong negative band north of the equator and the positive band at the equator indicate that ENSO in both models

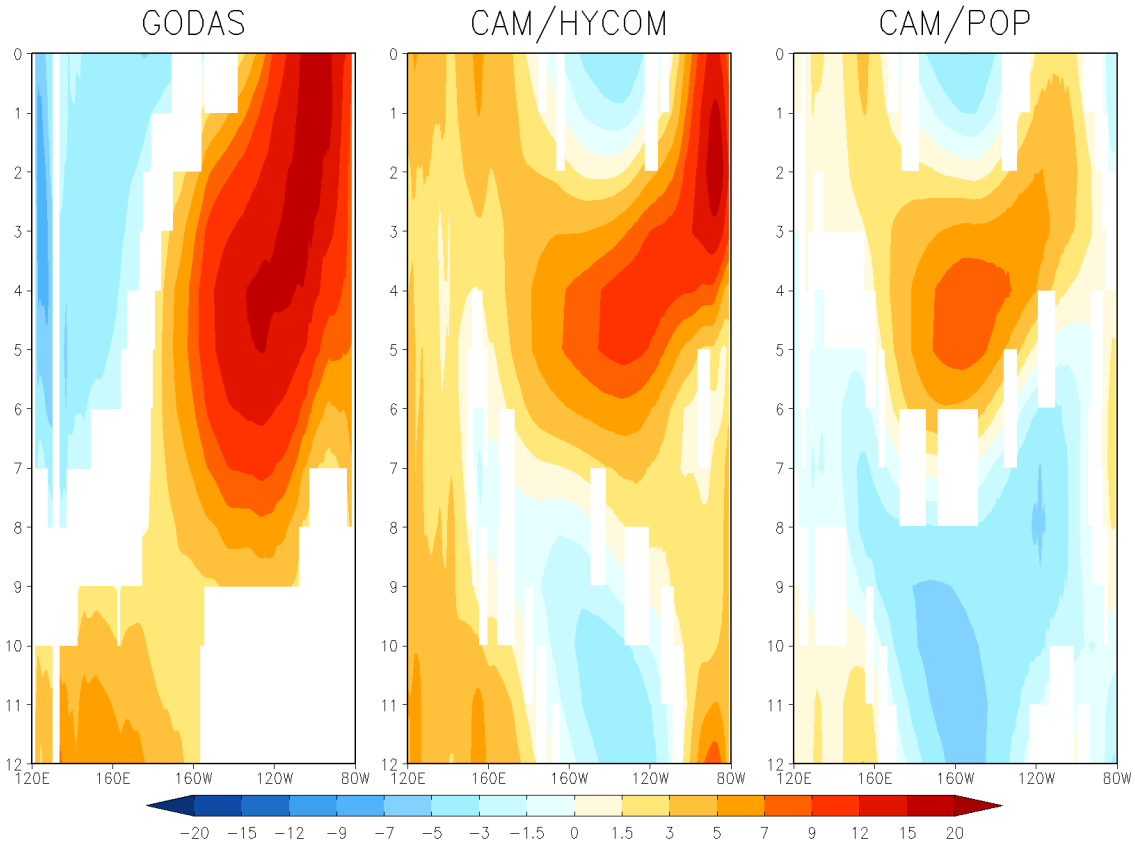

Figure 3.15: Lag-Regression of Niño 3 SST on Equatorial Thermocline Depth normalized by Niño 3 SST for a) ERSST, b) CAM-HYCOM, and c) CAM-POP. Values given in meters significant at 90% confidence limit. Positive lags Indicate Niño 3 SST lags Thermocline Depth.

modulate of the Hadley cell to a greater degree than observed. The modulation of the Hadley cell comes at the expense of proper Walker circulation variance.

Second, we examine the zonal wind stress related to ENSO. From theory (Jin 1997) and observations (Panel 'a' of Fig. 3.17) there is an expected slacking of the trades in the central and Western Pacific during a warm ENSO event and a strengthening during a cold event. In Fig. 3.17 positive values represent eastward stresses, a lull in the trade wind speed. By Jin (1997) we should expect the meridional span of wind stress anomalies to increase as the ENSO timescale increases. GODAS shows the anomalous region extending from 15°S to slightly above the equator. CAM-HYCOM and CAM-POP have a similar extent spanning a few degrees less than GODAS. Thus, the time scale of ENSO in both models can be explained as a shorter recharge/discharge phase than observed. Additionally, the strength of ENSO in these models is comparatively weaker than observed since the charging of WWV is less.

3.7 SST Tendency Equation

Correlating the time derivative of the Niño 3 SST with the various terms of the SST anomaly equation provides the source of temperature anomalies associated with ENSO events. The aim of this is not to estimate the budget of SST but rather to evaluate the relative importance of the advective terms in the SST equation. Using an intermediate coupled model, Battisti (1988) showed that the leading term in the SST equations is the meridional advection over Central East Pacific and vertical advection in the East Pacific.

Fig. 3.18 shows that the vertical advection contributes to the SST tendency whereas the meridional terms act to diffuse the anomaly away from the equator in GODAS. The temperature anomaly advected zonally in the east correlates with Niño

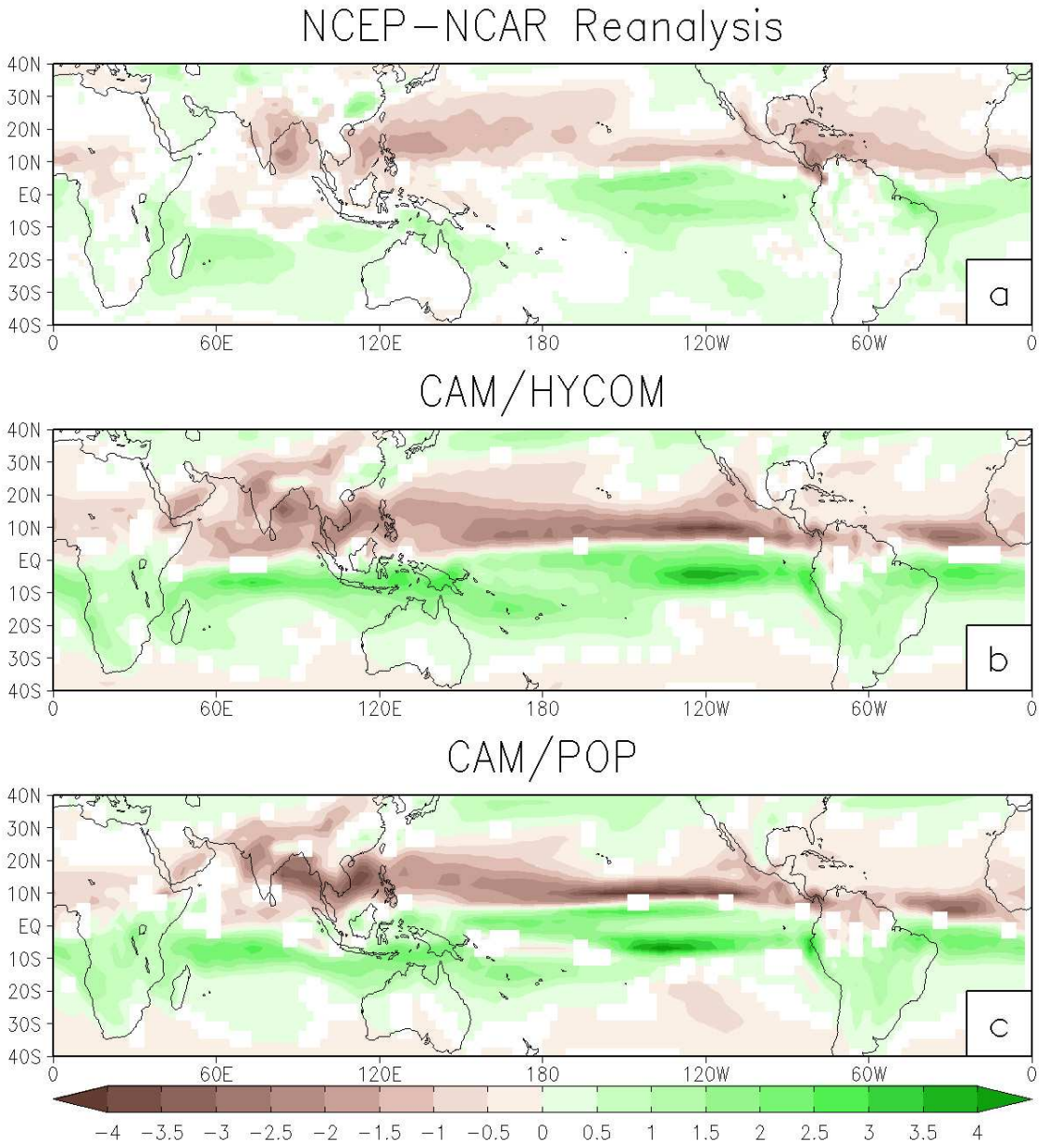

Figure 3.16: Regression of Niño 3 Index on Precipitation in mm per day normalized by Niño 3 SST for a) NCEP-NCAR Reanalysis, b) CAM-HYCOM, and c) CAM-POP. Only values significant at 95% confidence limit are plotted.

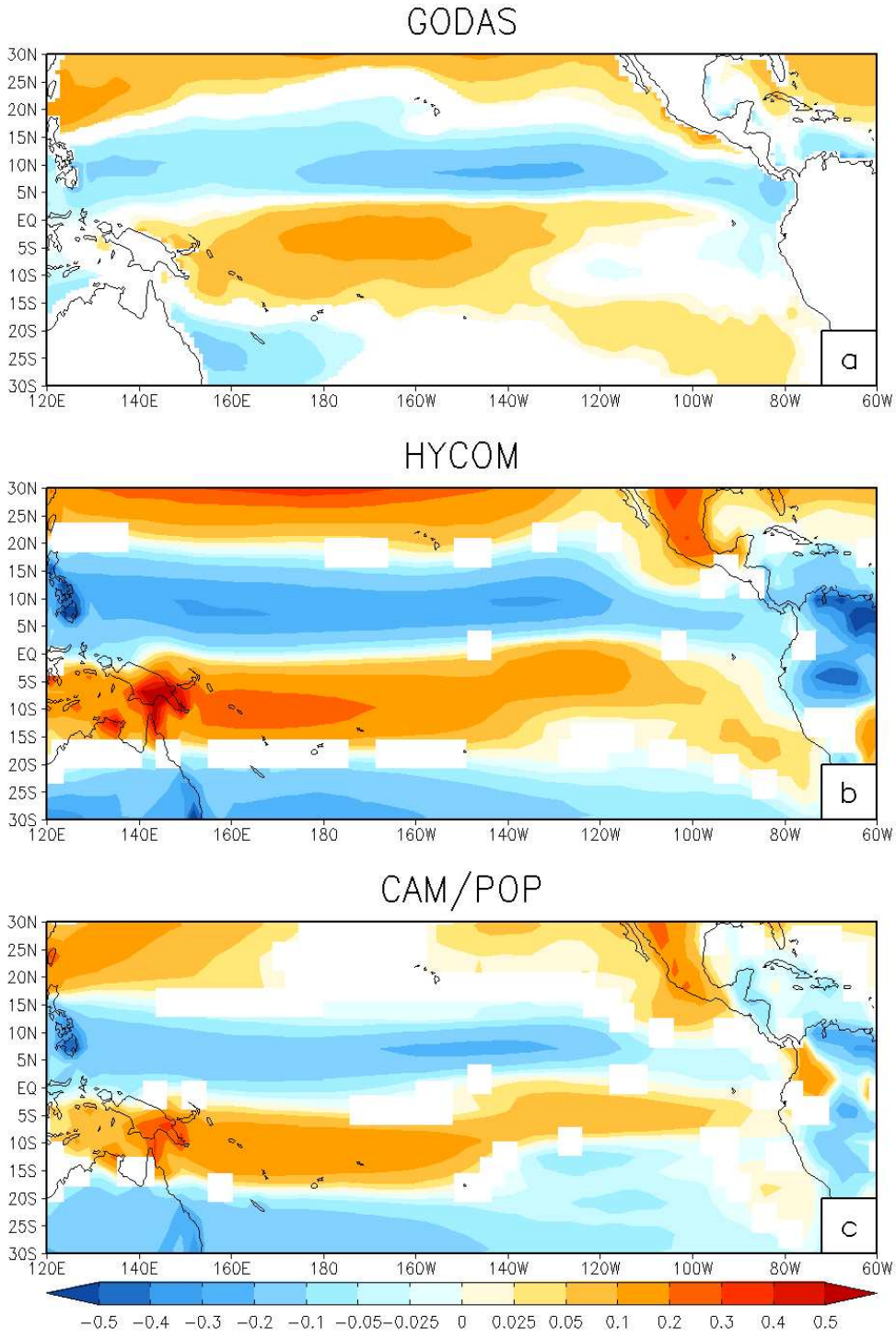

Figure 3.17: Regression of Niño 3 Index on Zonal Wind Stress in dynes per square cm normalized by Niño 3 SST for a) NCEP-NCAR Reanalysis, b) CAM-HYCOM, and c) CAM-POP. Only values significant at 95% confidence limit are plotted.

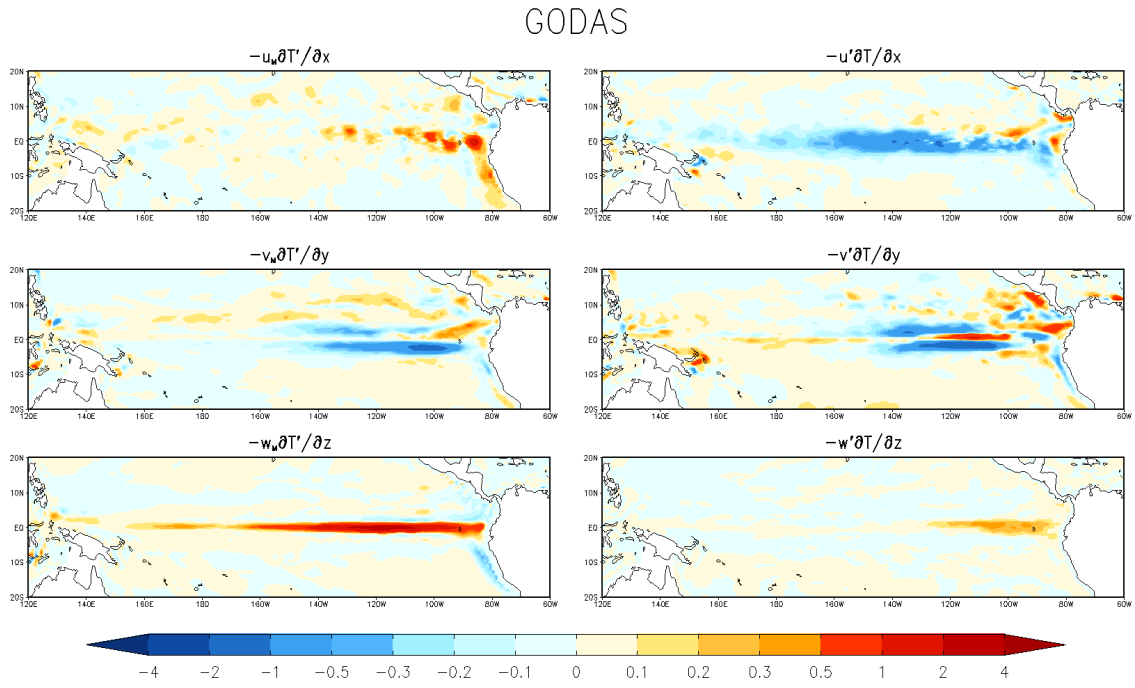

Figure 3.18: Covariance of Niño 3 SST tendency with advective terms of the SST anaomaly equation normalized by the Niño 3 SST tendency for GODAS.

3 SST tendency but the anomalous zonal advections has a negative relationship with the SST tendency.

Because GODAS uses the ocean model MOM, a model similar to CAM-POP, the possibility exists that results from this type of study could reflect the similarities in ocean models. To gain perspective on model physics parallels, CFS twentieth century control run was used also. This CFS control run does not assimilate any observations and is used for the purpose of verifying results - not for validating CAM-HYCOM or CAM-POP. CFS was chosen because of the top-class ENSO simulation in this coupled model (Wang et al. 2005) and the use of MOM as the ocean model. In Fig. 3.19 the dominant term is the mean vertical advection of anomalous temperature. The correlations found in CFS are of the same sign as seen in GODAS with the exception

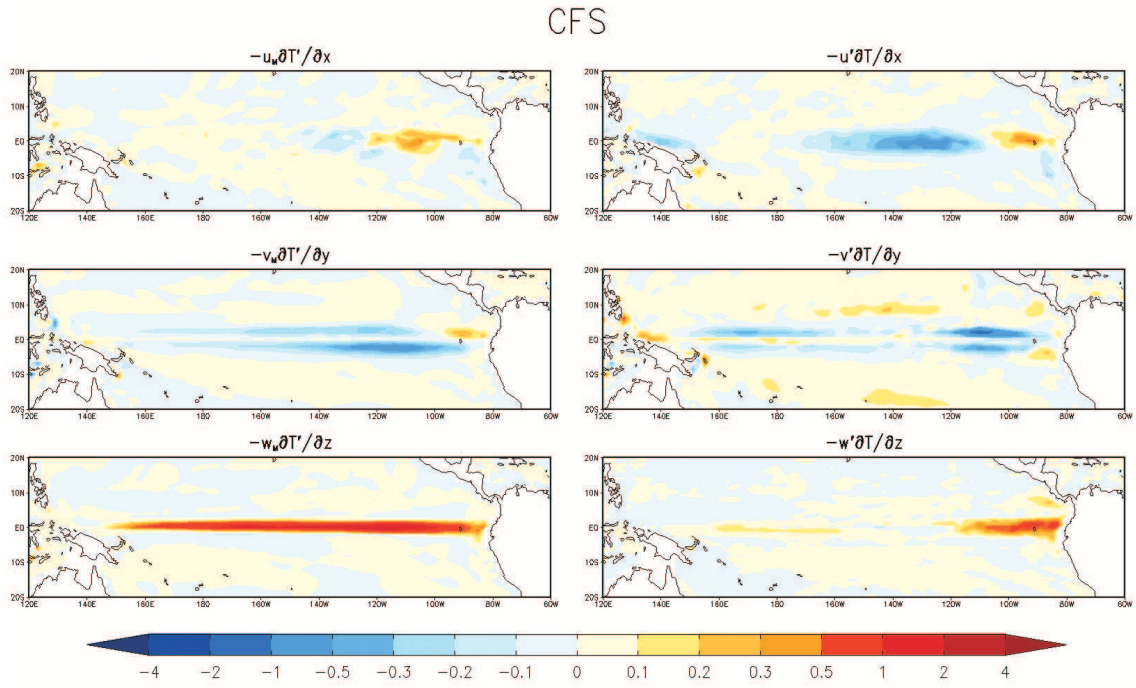

Figure 3.19: Same as Fig. 3.18 but for CFS.

of anomalous zonal advection in the far Eastern Pacific. The meridional advection terms show a similar pattern as seen in GODAS but with lower magnitude in relation to vertical advection.

The results for CAM-HYCOM given in Fig. 3.20 suggest that the dominant term is mean vertical advection in the central East Pacific and zonal anomalous advection in the far East Pacific. The meridional terms show little correlation to the time derivative of SSTs most likely because of the weak ENSO strength in CAM-HYCOM. In CAM-POP (Fig. 3.21) the correlation values are more robust that in CAM-HYCOM and the meridional terms are present. In CAM-POP there appear two flaws not seen in CAM-HYCOM or CFS: the correlation with anomalous vertical advection is negative and the correlation with anomalous zonal advection in central Pacific is moderately weak.

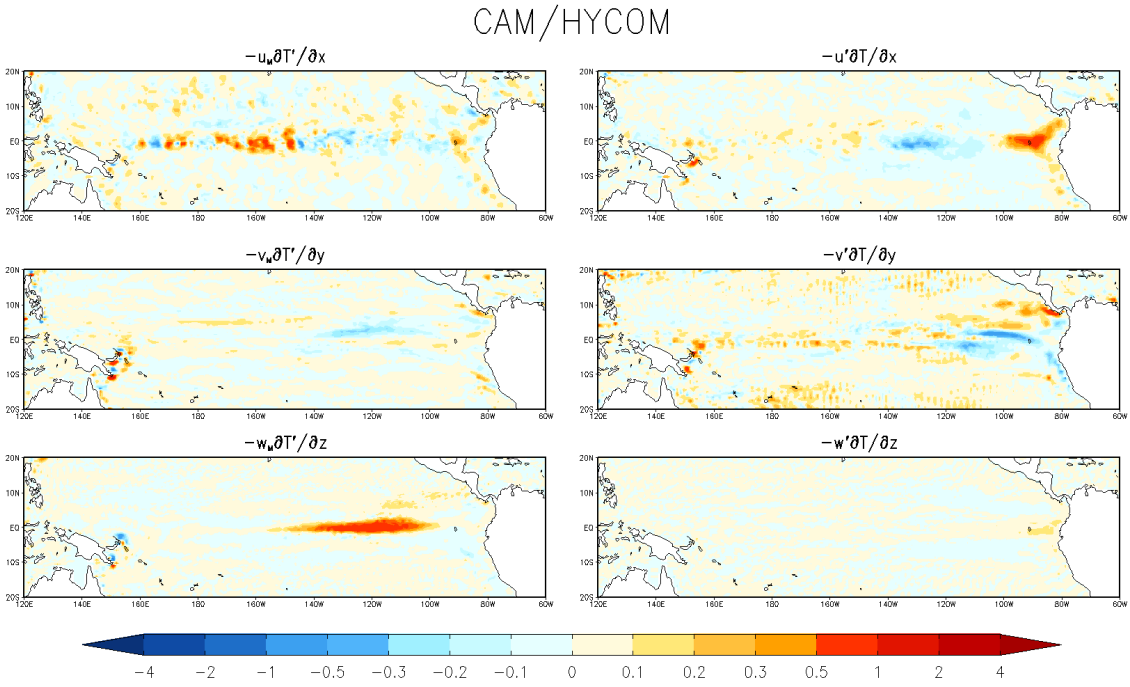

Figure 3.20: Same as Fig. 3.18 but for CAM-HYCOM.

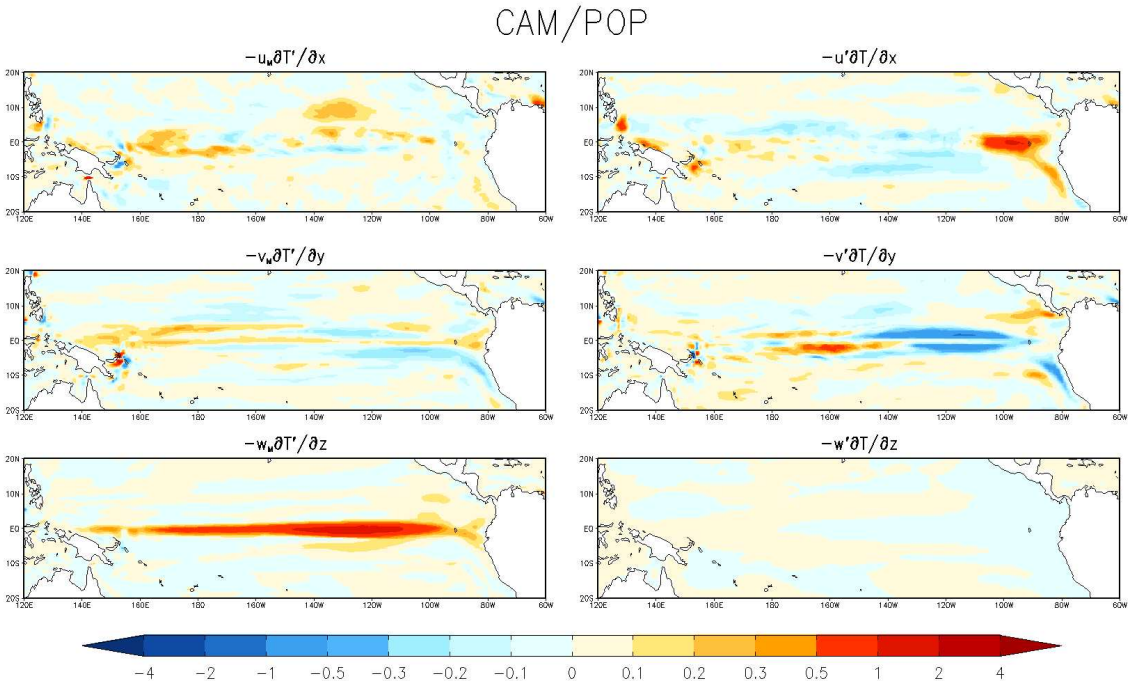

Figure 3.21: Same as Fig. 3.18 but for CAM-POP.

The surface currents in CAM-POP are acting fundamentally different from those in CAM-HYCOM. Even though the atmospheric winds behave similarly in both CAM-HYCOM and CAM-POP, the ocean response in CAM-POP does not produce the proper upwelling in the Eastern Pacific seen in GODAS, CFS, and CAM-HYCOM. This might explain the zonal extent of ENSO variability in CAM-POP versus CAM-HYCOM.

Examination of the SST anomaly equation at lag-correlation with the SST tendency is needed to explain the evolution of ENSO events within this paradigm. Fig. 3.22 shows the covariance of Niño 3 SST tendency with each advective term at various lags for GODAS. Six months prior to peak SST change, the mean vertical advection term begins to positively influence the SST in the Pacific East of 160° W. In less than 3 months after, the reversal of SST anomalies occurs gradually for about one year. The mean zonal advection of anomalous temperature, the term responsible for the horse shoe pattern in the West Pacific, is also significant at three to six months lead/lag.

The CFS control run (Fig. 3.23) differs from GODAS in that the mean vertical advection term starts positively affecting the Pacific almost nine months prior and has a gradual westward progression across the Pacific basin. CFS also lacks any strong pattern in the Western Pacific for the mean zonal advection term. There also appears to be a lag-covariance with anomalous vertical velocities much stronger than in GODAS.

In the CAM-HYCOM coupled model most advection terms have little significance besides mean vertical advection (Fig. 3.24). Notably, at 15 months lag the reverse correlation is seen in the mean vertical advection term likely because of a regular return period in CAM-HYCOM. CAM-POP Fig. 3.25 has a very similar response compared to CFS with the exception of the anomalous vertical velocity noted previ-

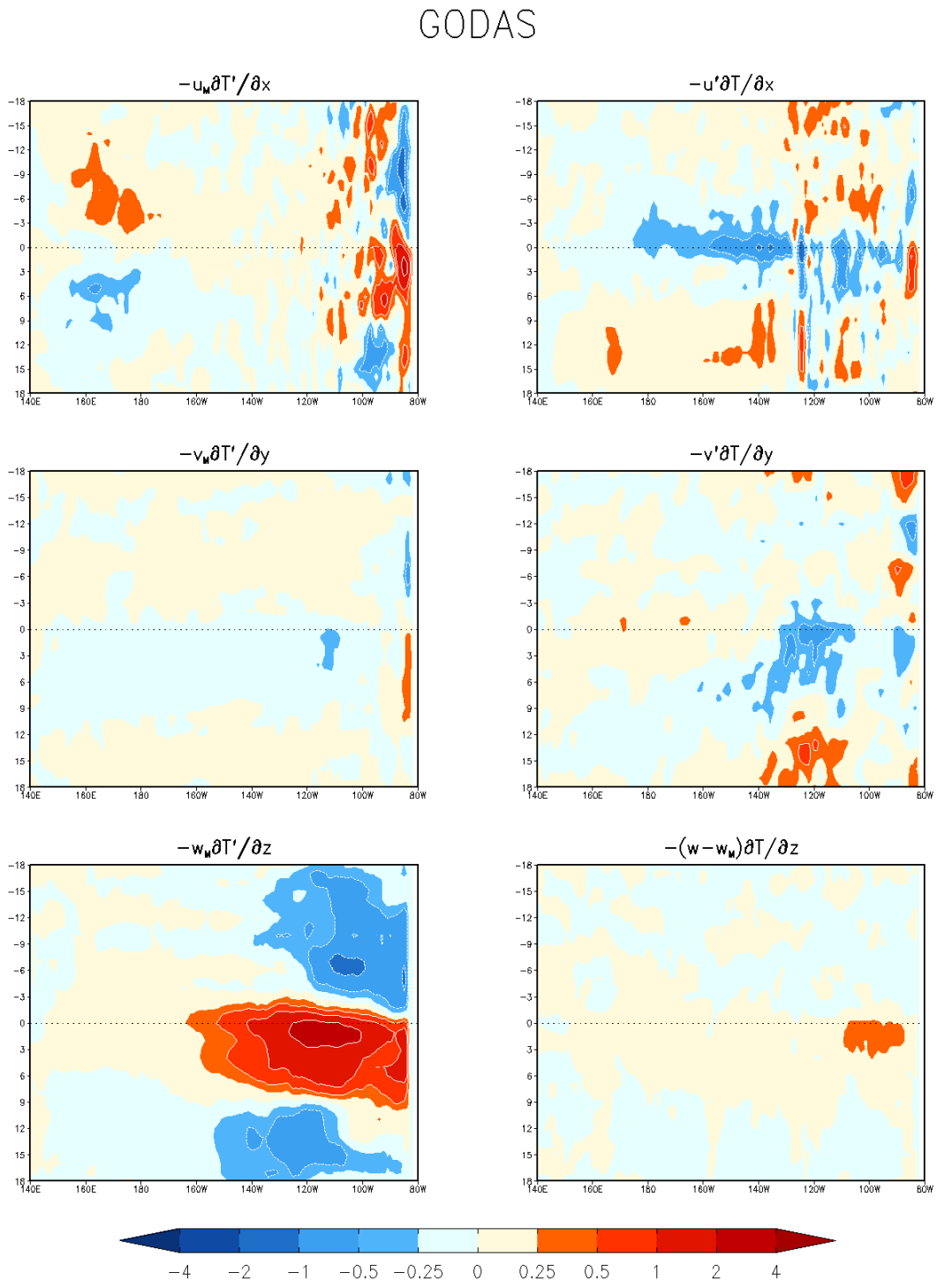

Figure 3.22: Hovmöller diagram showing equatorial lag-covariance of Niño 3 SST tendency with advective terms of the SST anaomaly equation normalized by the Niño 3 SST tendency for GODAS.

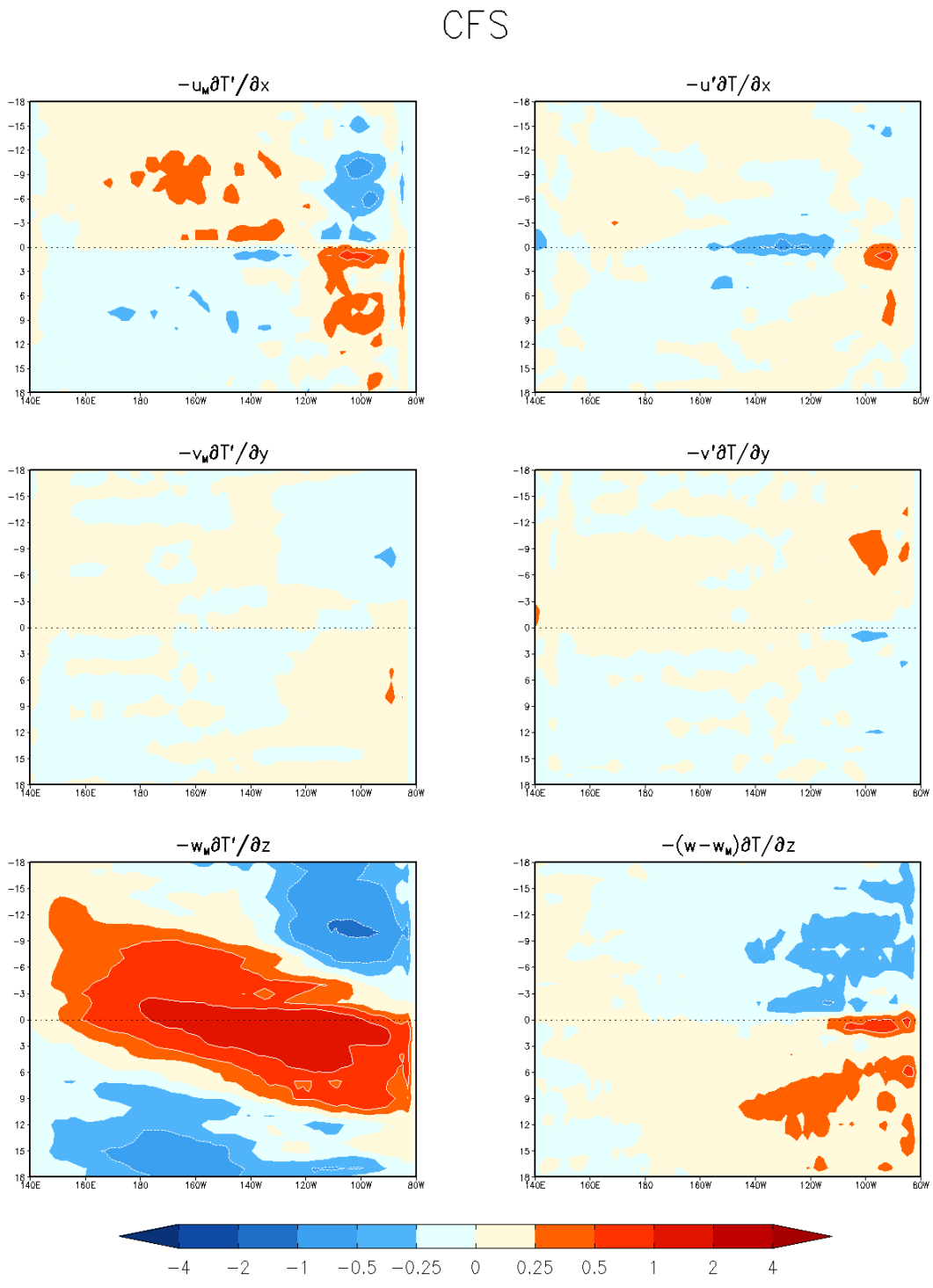

Figure 3.23: Same as Fig. 3.22 but for CFS.

ously. Mean vertical advection covariance with SST tendency has the same westward propagation as seen in CFS, but the biennial oscillation is clear in CAM-POP.

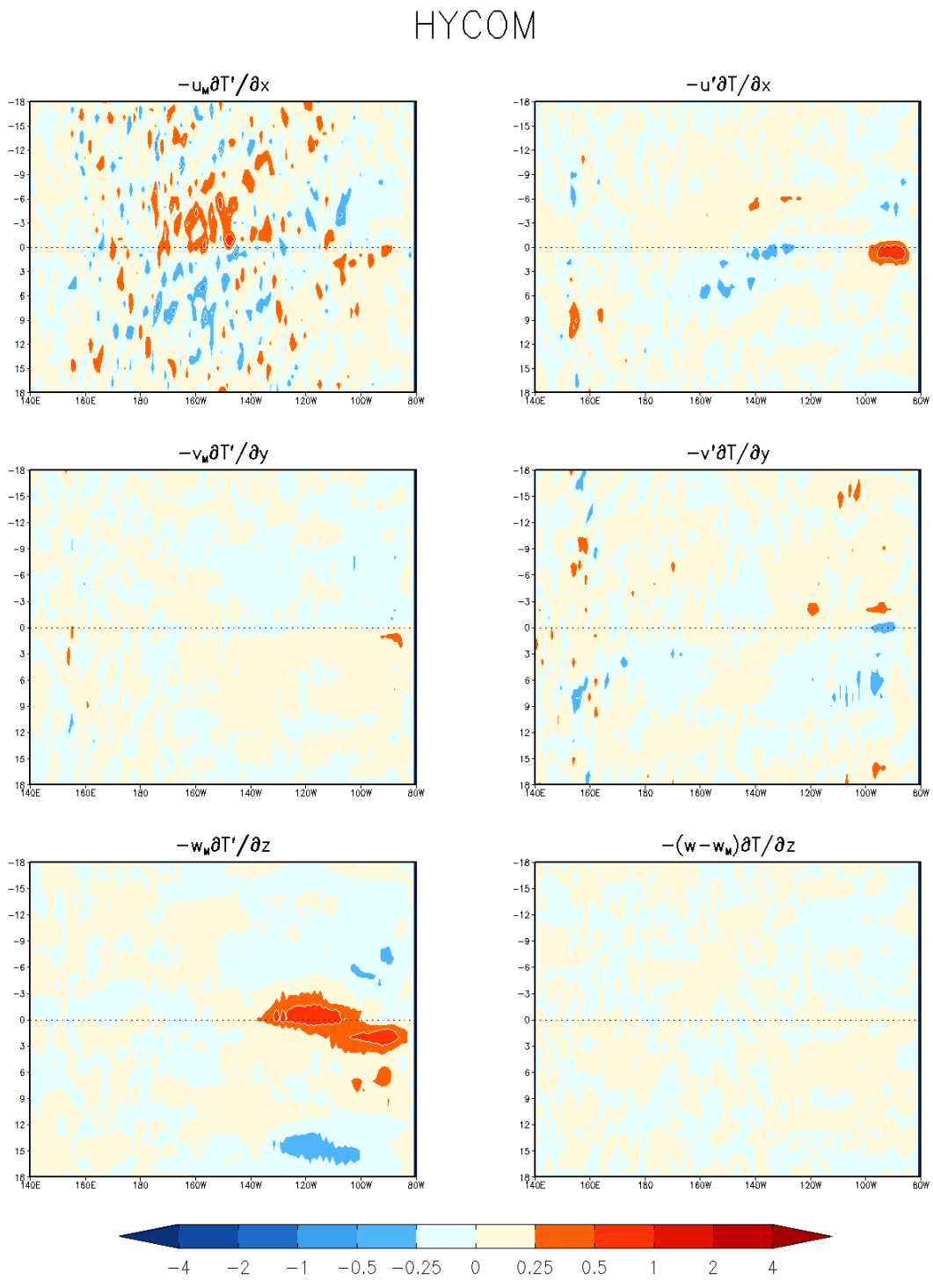

Figure 3.24: Same as Fig. 3.22 but for CAM-HYCOM.

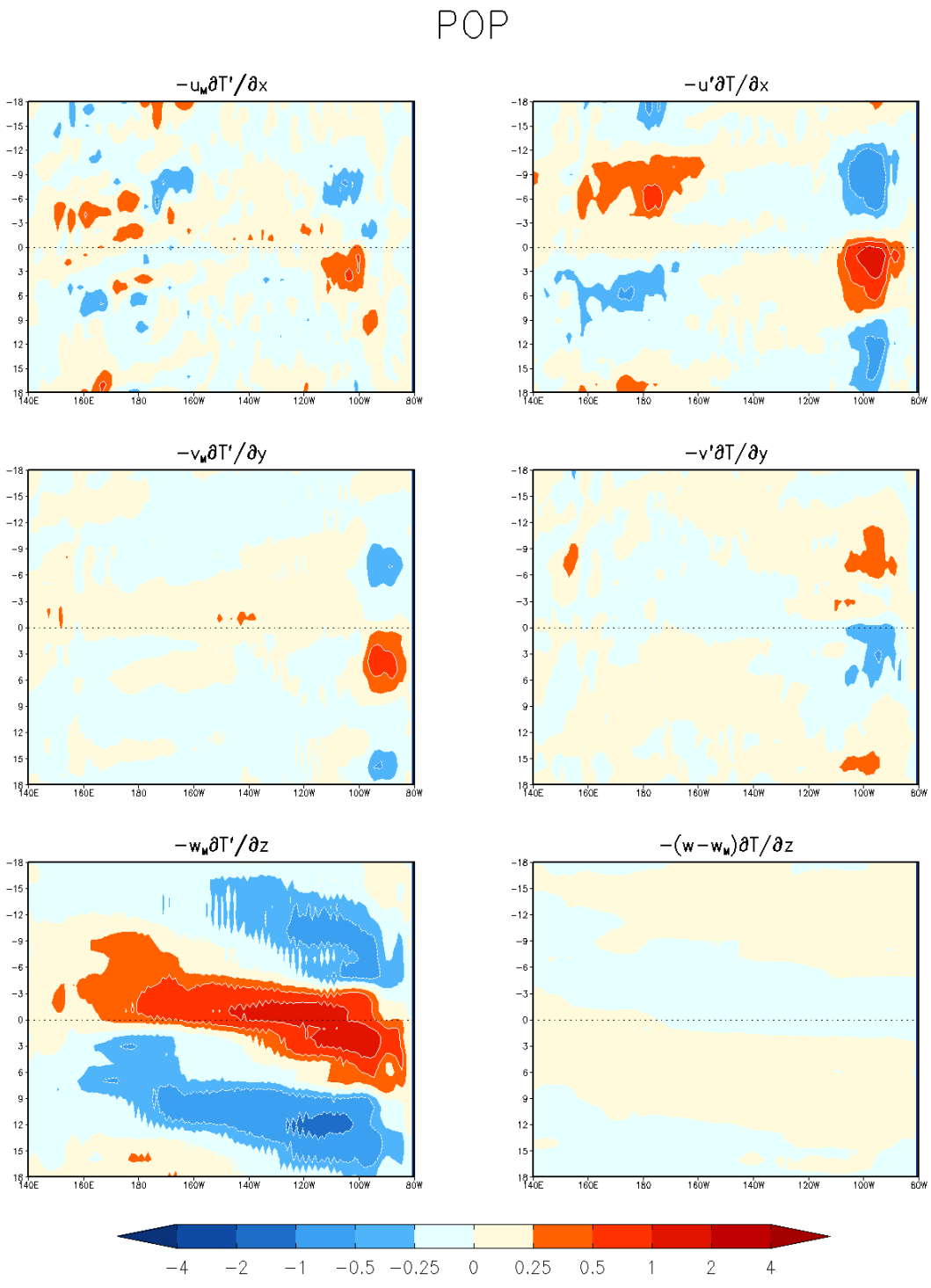

Figure 3.25: Same as Fig. 3.22 but for CAM-POP.

CHAPTER 4

CONCLUSION

Compared to ERSST, the return period of ENSO in CAM-HYCOM and CAM-POP is slightly shorter and the power is less than half. The power spectrum reveals the large erroneous biennial signal of Niño 3 SST in CAM-POP that is not seen in observations. The biennial oscillation in CAM-POP accounts for a majority of the variance in the equatorial Pacific SST in that model. The duration of ENSO events in both CAM-HYCOM and CAM-POP is slightly shorter than in ERSST.

The seasonal cycle of zonal wind stress and SST (Gill's seasonal cycle) in the equatorial Pacific shows only slight change between the two coupled models examined, CAM-HYCOM and CAM-POP. Because of the deviation in CAM-HYCOM and CAM-POP from the observed seasonal cycle, the physical mechanism behind the seasonal phase-locking of ENSO is not present. The apparent phase-locking of ENSO in CAM-POP is attributed to the regularity of the biennial oscillation and not to the seasonal changes in winds over the Central Pacific.

For both CAM-HYCOM and CAM-POP, the atmospheric behavior related to warming/cooling in the East Equatorial Pacific is about the same. When comparing the atmospheric feedbacks to ENSO (precipitation and wind stress), both simulations displayed similar spatial patterns to each other. For precipitation, the modulation of the Walker circulation as shown by the regression of Niño 3 SST on precipitation

in the NCEP-NCAR Reanalysis were not present in CAM-HYCOM or CAM-POP. Likewise, changes in zonal wind stress associated with ENSO (anomalous winds over the Central Pacific, extending pole-ward from the equator) were incorrect in both models. Instead of a centrally located area of anomalous winds, the entire Equatorial Pacific contained anomalies in a narrow band; this is consistent with the pattern seen for precipitation. Together the errors in precipitation and wind stress emphasize the poor representation of ENSO both models.

The overall low Niño 3 variance in CAM-HYCOM is most likely caused by a lack of cold water upwelling in that model. The tilt of the thermocline in CAM-HYCOM is weaker than in CAM-POP or GODAS. In the Eastern Pacific the mean thermocline depth in CAM-POP is sufficient such that anomalous conditions trigger high variance SST over that region. The feedbacks present in the CAM-POP coupled system cause a majority of this variance to occur regularly on a 2-year cycle. If the thermocline representation in CAM-HYCOM were improved, additional interannual variance might exist.

Analysis of spatial extent of the ENSO SST variance shows that CAM-HYCOM is a better fit to observed ENSO than CAM-POP. The spatial structure of ENSO in CAM-POP is thin and elongated, extending across the entire Pacific basin. In CAM-HYCOM, the spatial structure of ENSO is limited to the Eastern half of the Pacific coming to a point at the equator in the Central Pacific similar to the structure displayed in the ERSST dataset. For both CAM-HYCOM and CAM-POP, the variance in the coastal Eastern Pacific does not match that of ERSST.

Analysis of spatial extent of the biennial SST variance provides evidence for disappearance of the strong biennial oscillation in CAM-HYCOM. In CAM-POP, the spatial structure of the biennial oscillation closely resembles the structure of CAM-POP's ENSO variance – elongated and confined to very near the equator. In CAM-HYCOM,

there is strong relationship of the two-year oscillation with the waters off the coast of Peru. The model differences between HYCOM and POP in the Peruvian coastal region are likely responsible for the absence of the biennial cycle in CAM-HYCOM. This is evident from the differences in the ENSO and biennial patterns seen in CAM-HYCOM versus CAM-POP. The high correlation of the Peruvian coastal waters with the biennial oscillation in CAM-HYCOM is probably caused by model diffusion; this implies that changes in the biennial oscillation are because of differences in OGCM diffusion.

Following the Delayed Oscillator paradigm, both CAM-HYCOM and CAM-POP show a response to upwelling and downwelling equatorial waves. The lag-correlation of thermocline depth with Niño 3 SST shows that equatorial waves influence the Central Pacific thermocline depth about 4-6 months prior to peak variance in the Eastern Pacific. The progression of the thermocline anomaly moves eastward until reaching the eastern boundary. This is about 2-3 months faster than expected when compared to GODAS. In CAM-POP, particularly, the biennial oscillation is forced by the progression of equatorial waves; this is supported by the action of the delayed oscillator.

Both CAM-POP and CAM-HYCOM appear to have correctly simulated the tilt mode and recharge-discharge mode of the thermocline. For ENSO time-scale variance the tilt mode seen in CAM-HYCOM and CAM-POP resembles that of GODAS. For other frequencies, the tilt of the thermocline played a role only in the Eastern Pacific; the recharge-discharge oscillator is not responsible for the biennial variance. The Niño 3 tendency in both coupled simulations maintained a relationship with thermocline depth consistent with theory as confirmed in GODAS.

The choice of OGCM for simulation of ENSO is important in many ways. As demonstrated with the comparison of CAM-HYCOM and CAM-POP, the choice of

OGCM can substantially change the reproduction of ENSO. In this particular configuration, changing the ocean model to HYCOM removed the biennial oscillation entirely. Other studies have shown that improvements to the atmospheric convection scheme in CAM-POP can remove the erroneous biennial signal. In the case of CAM-HYCOM, however, the diffusion in HYCOM is likely the cause for the absence of a strong biennial signal. Even so, the spatial patterns of ENSO are significantly different depending on the ocean model used.

In light of progress made in ENSO fidelity of CAM-POP by others, future work in coupling HYCOM to CCSM4.0 might provide additional insight. The latest revision in the coupled climate model CAM-POP (CCSM4.0/CESM1.0) has improved the simulation of ENSO considerably through improvements in atmospheric convection parameterization. With model data for four similar coupled models (CAM3-POP, CAM3-HYCOM, CAM4-POP, and CAM4-HYCOM) a deeper look into the importance of the OGCM on ENSO can be taken.

BIBLIOGRAPHY

Allan, R. J., J. Lindesay, and D. E. Parker, 1996: *El Niño - Southern Oscillation & Climatic Variability*. CSIRO Publishing, 405 pp.

Ashok, K., S. Behera, S. A. Rao, H. Weng, and T. Yamagata, 2007: El niño modoki and its possible teleconnection. *J. Geophys. Res.*, **112**, C11 007.

Barber, R. T. and F. P. Chavez, 1983: Biological consequences of el niño. *Science*, **222**, 1203–1210.

Battisti, D. S., 1988: Dynamics and thermodynamics of a warming event in a coupled tropical atmosphere-ocean model. *J. Atmos. Sci.*, **45**, 2889–2919.

Behringer, D. and Y. Xue, 2004: Evaluation of the global ocean data assimilation system at ncep: The pacific ocean. eighth symposium on integrated observing and assimilation systems for atmosphere, oceans, and land surface. *AMS 84th Annual Meeting*, Seattle, WA, 11–15.

Cane, M. A., 1983: Oceanographic events during el niño. *Science*, **222**, 1189–1195.

Capotondi, A., A. Wittenberg, and S. Masina, 2006: Spatial and temporal structure of tropical pacific interannual variability in 20th century coupled simulations. *Ocean Modeling*, **15**, 274–298.

Clarke, A. J., 2008: *Dynamics of El Niño & the Southern Oscillation*. Academic Press, 308 pp.

Clarke, A. J., S. V. Gorder, and G. Colantuono, 2007: Wind stress curl and enso discharge/recharge in the equatorial pacific. *J. Phys. Oceanogr.*, **37**, 1077–1091.

Diaz, H. F., M. P. Hoerling, and J. K. Eischeid, 2001: Enso variability, teleconnections and climate change. *Int. J. Climatol.*, **21**, 1845–1862.

Gadgil, S., P. V. Joseph, and N. V. Joshi, 1984: Ocean-atmosphere coupling over monsoon regions. *Nature*, **312**, 141–142.

Glantz, M. H., 2000: *Currents of Change: Impacts of El Niño and La Niña on Climate and Society*. 2d ed., Cambridge University Press, 266 pp.

Gray, W. M., 1984: Atlantic hurricane frequency. part i: El niño and 30mb quasi-biennial oscillation influences. *Mon. Wea. Rev.*, **112**, 1649–1668.

Guilyardi, E., A. Wittenberg, A. Fedorov, M. Collins, C. Wang, A. Capotondi, G. J. van Oldenborgh, and T. Stockdale, 2009: Understanding el niño in ocean-atmosphere general circulation models. *Bull. Amer. Meteor. Soc.*, **90**, 325–339.

Guilyiardi, E., 2006: El niño mean state-seasonal cycle interactions in a multimodel ensemble. *Clim. Dyn.*, **26**, 329348.

Halpert, M. S. and C. F. Ropelewki, 1992: Surface temperature patterns associated with the southern oscillation. *J. Climate*, **5**, 577–593.

Hanley, D. E., M. A. Bourassa, J. J. O'Brien, S. R. Smith, and E. R. Spade, 2003: A quantitative evaluation of enso indices. *J. Climate*, **16**, 1249–1258.

Hansen, J. W., A. W. Hodges, and J. W. Jones, 1998: Enso influences on agriculture in the southeastern united states. *J. Climate*, **11**, 404–411.

Hansen, J. W., A. W. Hodges, and J. W. Jones, 1999: El niño−southern oscillation impacts on winter vegetable production in florida. *J. Climate*, **12**, 92–102.

Hoerling, M. P. and A. Kumar, 2002: Atmospheric response patterns associated with tropical forcing. *J. Climate*, **15**, 2184–2203.

Hoerling, M. P., A. Kumar, and M. Zhong, 1997: El niño, la niña, and the nonlinearity of their teleconnections. *J. Climate*, **10**, 1769–1786.

Jin, F.-F., 1997: An equatorial ocean recharge paradigm for enso. part i: Conceptual model. *J. Atmos. Sci.*, **54**, 811–829.

Jolliffe, I. T., 2002: *Principal Component Analysis*. 2d ed., Springer, 520 pp.

Joseph, R. and S. Nigam, 2006: Enso evolution and teleconnections in ipccs twentieth-century climate simulations: Realistic representation? *J. Climate*, **19**, 4360–4377.

Kalnay, E., M. Kanamitsu, R. Kistler, W. Collins, D. Deaven, and co authors, 1996: The ncep/ncar 40-year reanalysis project. *Bull. Amer. Soc.*, **77**, 437471.

Kang, I.-S., I.-S. An, and F.-F. Jin, 2001: A systematic approximation of the sst anomaly equation for enso. *J. Meteor. Soc.*, **79**, 1–10.

Kao, H.-Y. and J.-Y. Yu, 2009: Contrasting eastern-pacific and central-pacific types of enso. *J. Climate*, **22**, 615–632.

Kim, H.-M., P. J. Webster, and J. A. Curry, 2009: Impact of shifting patterns of pacific ocean warming on north atlantic tropical cyclones. *Science*, **325**, 77–80.

Kistler, R., E. Kalnay, W. Collins, and S. Saha, 2001: The ncepncar 50-year reanalysis: Monthly means cd-rom and documentation. *Bull. Amer. Meteor. Soc.*, **82**, 247–268.

Li, T. and G. Philander, 1996: On the annual cycle in the eastern equatorial pacific. *J. Climate*, **9**, 29862998.

Misra, V., L. Marx, M. Fennessy, B. Kirtnman, and J. L. K. III, 2008: A comparison of climate prediction and simulation over the tropical pacific. *J. Climate*, **21**, 3601–3610.

Misra, V., L. Marx, J. L. K. III, and B. Kirtnman, 2007: Validating and understanding the enso simulation in two coupled climate models. *Tellus*, **59**, 292–308.

Neale, R. B., J. H. Richter, and M. Jochum, 2008: The impact of convection on enso: from a delayed oscillator to a series of events. *J. Climate*, **21**, 5904–5924.

Neelin, J. D., 1991: The slow sea surface temperature mode and the fast-wave limit: Analytic theory for tropical interannual oscillations and experiments in a hybrid coupled model. *J. Atmos. Sci.*, **48**, 584–606.

Pauly, D., P. Muck, J. Mendo, and I. Tsukayama, 1989: *The Peruvian upwelling ecosystem: dynamics and interactions*. Deutsche Gesellschaft für Technische Zusammenarbeit and International Center for Living Aquatic Resources Managment, 438 pp.

Penland, C., M. Ghil, and K. Weickmann, 1991: Adaptive filtering and maximum entropy spectra with application to changes in atmospheric angular momentum. *J. Geophys. Res.*, **96**, 422 659–22 671.

Philander, S. G., 1990: *El Niño, La Niña, and the Southern Oscillation*, International Geophysical Series, Vol. 46. Academic Press, 293 pp.

Rasmusson, E. M. and T. H. Carpenter, 1982: Variation in tropical sea surface surface temperature and surface wind fields associated with the southern oscillation/ el niño. *Mon. Wea. Rev.*, **110**, 354–384.

Ropelewki, C. F. and M. S. Halpert, 1987: Global and regional scale precipitation patterns associated with the el niño/southern oscillation. *Mon. Wea. Rev.*, **115**, 1606–1626.

Saha, S., et al., 2006: The ncep climate forecast system. *J. Climate*, **19**, 3483–3517.

Schneider, E. K., B. Huang, and R. Gudgel, 1995: Ocean wave dynamics and el niño. *J. Climate*, **8**, 2415–2439.

Schreiber, R. W. and E. A. Schreiber, 1984: Central pacific seabirds and the el niño southern oscillation: 1982 to 1983 perspectives. *Science*, **225**, 713–716.

Smith, T., R. Reynolds, T. C. Peterson, and J. Lawrimore, 2008: Improvements to noaa's historical merged land-ocean surface temperature analysis (1880-2006). *J. Climate*, **21**, 2283–2296.

Suarez, M. J. and P. S. Schopf, 1988: A delayed action oscillator for enso. *J. Atmos. Sci.*, **45**, 3283–3287.

Tang, B. H. and J. Neelin, 2004: Enso influence on atlantic hurricanes via tropospheric warming. *Geophysical Research Letters*, **31**.

Trenberth, K., 1997: The definition of el niño. *Bull. Amer. Meteor. Soc.*, **78**, 2771–2777.

Trenberth, K. E. and J. Guillemot, 1998: Evaluation of the atmospheric moisture and hydrological cycle in the ncep/ncar reanalyses. *Clim. Dynam.*, **14**, 213–231.

Trenberth, K. E. and T. J. Hoar, 1996: The 19901995 el niño-southern oscillation event: Longest on record. *Geophys. Res. Lett.*, **23**, 57–60.

Uppula, S. M., 2005: The era-40 re-analysis. *QUARTERLY JOURNAL OF THE ROYAL METEOROLOGICAL SOCIETY*, **131**, 29613012.

Wang, C., 2001: A unified oscillator model for the el niño-southern oscillation. *J. Climate*, **14**, 98–115.

Wang, W., S. Saha, H.-L. Pan, S. Nadiga, and G. White, 2005: Simulation of enso in the new ncep coupled forecast system model (cfs03). *Mon. Wea. Rev.*, **133**, 1575–1593.

Weare, B. C., 1986: An extension of an el niño index. *Mon. Wea. Rev.*, **114**, 644–647.

Wu, Z. and N. E. Huang, 2009: Ensemble empirical mode decomposition: A noise assisted data analysis method. *Advances in Adaptive Data Analysis*, **1**, 1–41.

Yang, H. and F. Wang, 2009: A revisit on the thermocline depth in the equatorial pacific. *Mon. Wea. Rev.*, **133**, 1575–1593.

Yu, J.-Y. and H.-Y. Kao, 2007: Decadal changes of enso persistence barrier in sst and ocean heat content indices. *J. Geophys. Res.*, **112**, 1958–2001.

Yu., J.-Y., F. Sun, and H.-Y. Kao, 2007: Contributions of indian ocean and monsoon biases to the excessive biennial enso in ccsm3. *J. Climate*, **22**, 1850–1858.

BIOGRAPHICAL SKETCH